Development of a motion guidance device for 4D CT scans of the wrist

BM51035: MSc-Thesis

W.H.A. Crezee

Delft University of Technology

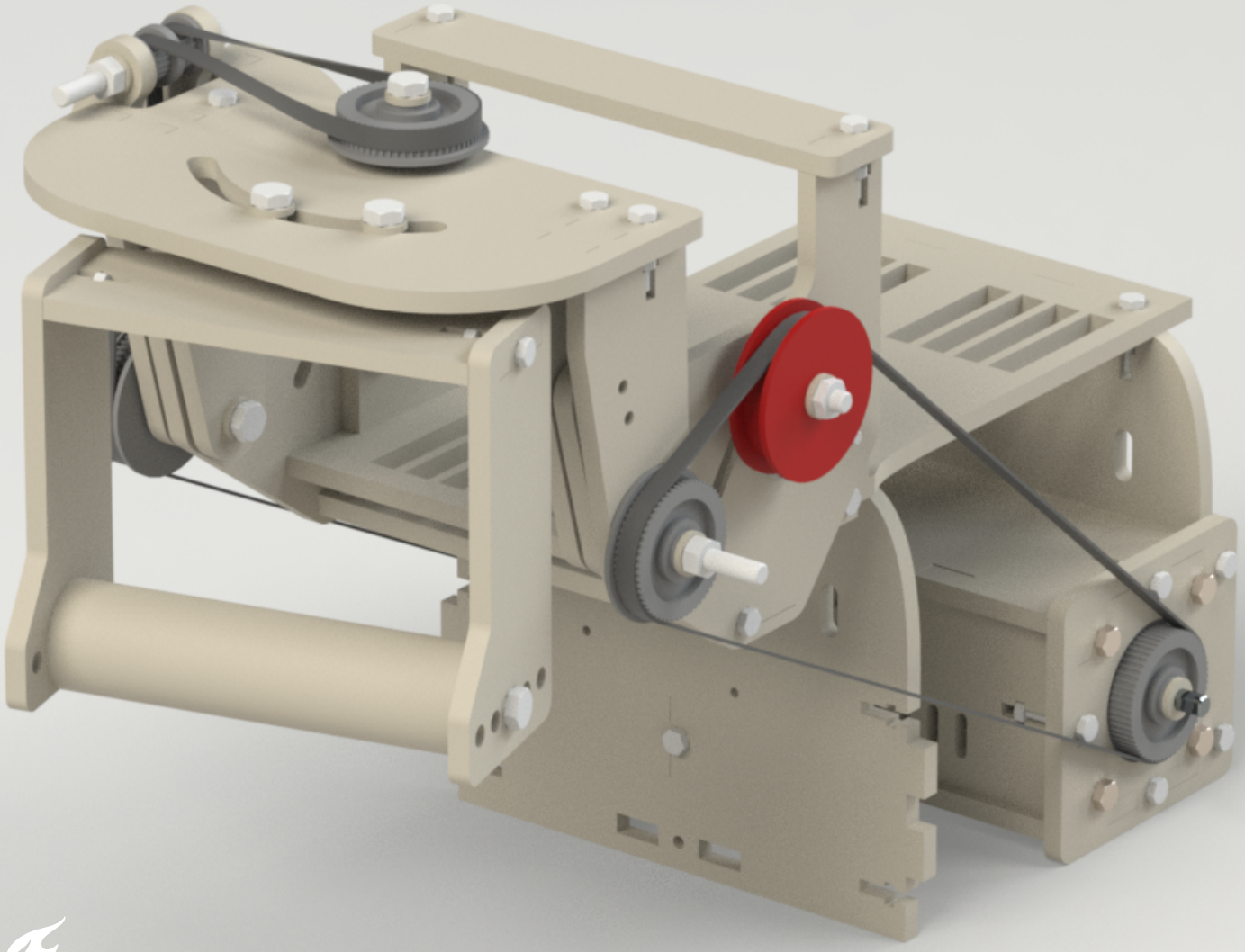

TU Delft

Development of a motion guidance device for 4D CT scans of the wrist

by

W.H.A. Crezee

to obtain the degree of Master of Science
at the Delft University of Technology,
to be defended publicly on 19-12-2022.

Student number:	4567218	
Project duration:	12/2021 – 12/2022	
Thesis committee:	Dr. Ir. N. Tümer,	TU Delft, supervisor
	Dr. G. A. Kraan,	Reinier Haga Orthopedisch Centrum
	Prof. dr. A. A. Zadpoor,	TU Delft

TU Delft

Preface

This master thesis describes the work I did to graduate with the master of BioMedical Engineering at the Technical University of Delft. This thesis has been worked on very hard for a long time, and it is my final assignment to hand in for my education in Delft. In this work, I describe the development of a motion guidance device for the wrist. This device can be used in conjunction with a 4D CT scanner to achieve reliable, moving images of the carpal bones in the wrist.

During this thesis, I had the opportunity to work at the research group of the Reinier Haga Orthopedisch Centrum in Zoetermeer. Here, I got to work with, and very close to surgeons, nurses, researchers and patients. I attended multiple surgeries and polyclinics. This internship has given me invaluable experience in working in a clinical setting, very close to the medical action.

I could never have completed this thesis without the help and contribution of several people. I would like to thank Dr. Ir. Nazli Tümer for her support and feedback. Our (almost) weekly meetings were always a welcome break in the week for reflection on what was done and looking at what had to be done. Next, I would like to thank Dr. Gerald Kraan for his everpresent enthusiasm, nonstop positivity and expert knowledge, and of course for all the clinical experience I got while working with him. Furthermore, I am extremely thankful for the guidance, feedback and overall very warm interactions with Dr. Johan van der Stok, and Dr. Nina Mathijssen. In performing the CT scans and determining the scan protocols, the expert knowledge of Ian Blom was invaluable. Likewise, the support I got from Ir. Sander Leeflang helped immensely in achieving the design of the wrist guidance device. For the cadaver experiment, I would like to thank Lucas Verdonschel of the Wetlab EMC, which provided the cadaveric specimens. Furthermore, I would like to thank Alex Ratschat, who helped me with the selection of the right motor unit. Finally, I am so grateful for the support from my wife Jetske, who has been my mainstay during the past year. Without her loving encouragement and questions, this thesis would not have been what it has become.

W.H.A. Crezee
Delft, December 2022

Contents

Nomenclature

Abbreviations

Abbreviation	Definition
CT	Computed Tomography
DISI	Dorsal Intercalated Segmental Instability
FE	Flexion-Extension
ICI	Intercarpal Instability
MCI	Midcarpal Instability
MRI	Magnetic Resonance Imaging
RHOC	Reinier Haga Orthopedisch Centrum
RUD	Radioulnar Deviation

List of Figures

List of Tables

1

Summary

This thesis presents the development of a motion guidance device for the wrist, meant to be used in combination with 4D CT scanning. This new, but still largely experimental, imaging technique is believed to show great potential. It could provide insight in the unrevealed kinematics of the wrist, but could also be of great diagnostic value. However, 4D CT scanning lacks standardization. To combat motion artefacts and other problems, it is important to have a smooth and standardized motion. This calls for a motion guidance device which can be used inside a CT scanner.

In this thesis, the development of such a device is described, as well as an experiment and analysis to validate the reliability of images made in combination with this device. The case of wrist instability is used to validate the device. A more elaborate explanation on wrist instability and substantiation of the problem can be found in chapter 2.

First, previous versions of a motion guidance device were analysed, and design criteria were set in collaboration with medical specialists. Then, an iterative design process followed, where new parts would be manufactured and introduced to the device, after which they were tested for their fit and use. After the design process, an experiment with three cadaveric samples was designed. This experiment consisted of sevaral 4D CT scans, six of each specimen. Motion speed, type of motion and radiation dosage were varied in these scans. After the scans were taken, they were analysed by three observers. These observers would measure lunate, scaphoid and capitate angles. These angles are important to the diagnosis of wrist instability. These measurements were then collected and both intra- and inter-observer agreement was calculated with the intraclass correlation coefficient (ICC). The methodology of both design, experiments and analysis can be found in chapter 3.

The result of the design process is a motorized motion guidance device which can perform both flexion/extension and ulnar/radial deviation in a 4D CT environment. It is driven with two timing belt arrays, powered by two stepper motors, and controlled by an Arduino microcontroller. This device succesfully performed the cadaveric experiments. Lunate, scaphoid and capitate angles were measured and analyzed. One specimen proved too stiff to move significant amounts, so its data was excluded from analysis. Both intra- and inter-observer agreement were good to excellent, except for a few measurements, notably the schaphoid with low radiation dosage. The results of the design process, experiments and analysis can be found in chapter 4.

While there are some design optimalizations that can be implemented, the overall design of the motion guidance device is very functional and it succesfully performed the cadaveric experiments. When compared with literature, reported ICC values for similar measurements are very comparable to values found in this thesis. It is important to note however that all ICC values that were lower were of measurements of the scaphoid. This can be explained due to the complex anatomy of this particular in combination with lower visibility during low dosage scans. Further analysis, design optimalizations, limitations of the study and recommendations can be found in chapter 5.

Chapter 6 provides a conclusion to the thesis. In short, this thesis describes the development of a succesfull motion guidance device to be used in combination with a 4D CT scanner. The scans produced in combination with this device provide images which can be used to measure clinically important angles reliably. In the future, these kind of devices can be used for analysis of carpal kinematics, evaluation of carpal prosthetics, or in clinical diagnostic settings.

2 Introduction

This thesis will describe the development of a motion guidance device for the wrist. The guidance device is meant to be used in combination with a 4D CT scanner. Being able to study motion can provide insight into the kinematics of the wrist, as well as be of diagnostic value in clinical applications. This thesis study was performed in collaboration with the research group at the Reinier Haga Orthopedisch Centrum (RHOC).

2.1. Motivation

As one of the most complex joints in the human body, the wrist offers unrevealed kinematics between carpal bones, ligaments and other tissues. These kinematics are not well understood and cannot be imaged well by traditional imaging methods such as two-dimensional X-ray and magnetic resonance imaging (MRI) [1–3]. A quantitative method of imaging the carpal bones in motion is needed to better understand the kinematics of the wrist, as well as provide significant clinical value. In the literature, there seems to be no consensus on the best imaging technique to study wrist kinematics [1, 4–8]. An earlier completed literature review on dynamic imaging techniques by the same author as this thesis analysed 70 scientific publications. In this review, seven imaging techniques used to scan the wrist under dynamic conditions are compared. Based on different factors, including accuracy, harm to the patient or damage to the specimen, and sample rate, 4-dimensional computed tomography (4D CT) is stated as being most proficient in measuring wrist kinematics. Hence, this thesis will focus on 4D CT scanning as an imaging technique to image the wrist under dynamic conditions.

When looking at the literature, 4D CT scanning for the wrist is mostly an experimental technique, not yet used in clinical settings. Although its relevance and potential are widely accepted, its use is often still experimental [3, 9–11]. One problem which was noted during the writing of the literature review and during numerous conversations with specialists is the lack of standardization in 4D CT scans [5, 12]. In the case of experiments on live participants, the scan is often made of a hand which is simply held in the scanning region of the CT scanner and then moved around [13, 14]. Other studies build a customized motion rig which guides wrist motion and limits out-of-plane movements [15]. There is also no standard way of moving cadaveric specimens in 4D CT experiments. Specimens are moved in a number of ways, from mechanically pushing fingers to impose thumb opposition [7], to passively moving the hand with a motion device [16]. This lack of standardization raises several problems. First, moving during a CT scan brings new variables into play. These variables, such as movement speed, make it hard to assign clinical value to the measurements without any kind of reference. One can imagine a 4D CT scan as a series of photographs made of a moving object. Just like in photography, this can result in blurry images. These ”motion artefacts” are very prevalent and result in less reliable images. Second, comparing different scans with each other is more complex with a lack of standardization. Moreover, comparing results between different studies is even more difficult. The use of a documented standardized device would help greatly in solving these issues.

This lack of standardized movement is the main inspiration for the goal of this thesis. As noted above, several studies have been done using some specialized motion rigs. However, these motion rigs are seldom well-described and validated. Little is known about their performance and development

process, while these kinds of devices can be very beneficial, both in experimental settings, as well as clinical settings. One example is the diagnosis of dynamic wrist instability, which currently uses unreliable diagnostic methods [17]. This example will be discussed in more detail in section 2.2, as it will be used as a case to validate the designed motion device. Another example is the development of 3D-printed lunate implants for patients with Kienböck disease, a degenerative condition of the lunate bone. Standardized kinematic data is needed to validate the kinematics of the implanted bones. Lastly, as said before, wrist kinematics are not well understood. Standardized motion studied with 4D CT scans might provide critical insight into the complex kinematics of the carpal bones.

2.2. Case: Dynamic carpal Instability

To validate the motion guidance device, dynamic carpal instability is used as a case. When talking about instability in this work, dynamic instability, wrist instability, carpal instability and dynamic carpal instability can all be used interchangeably.

Carpal instability is a term which houses many types of instabilities. Because of the complex anatomy and biomechanics of the wrist, it is a difficult-to-diagnose disorder which mainly relies on static conventional imaging methods. Many forms of carpal instability exist, some of which show abnormal findings on only very specific views of medical images, or show them in a much later stage [18, 19]. Delayed diagnosis can lead to adverse effects such as osteoarthritis. However, the diagnosis often still relies on conventional, static imaging techniques such as plain radiographs, MRI, and fluoroscopy. With the limited reliability and accuracy of these static imaging techniques, many specialists consider wrist arthroscopy the golden standard in diagnosing wrist instabilities [20–22]. In this invasive and often expensive procedure, one or more small incisions are made in the wrist, through which a tube with a camera is inserted. This allows a surgeon to view the inside of the wrist in static and moving conditions. For carpal instability, the Geissler grading system is usually utilized as a classification method [23]. However, as recently shown in an international study with 60 surgeons, the interobserver agreement of diagnostic wrist arthroscopy using this classification method is poor [17]. The fact that the accepted golden standard for carpal instability seems to have poor interobserver agreement presents a hiatus in diagnosing carpal instability. If arthroscopy is inadequate, no satisfactory method exists to diagnose carpal instability. A non-invasive method which can give insight into wrist kinematics in dynamic conditions could be of great benefit.

In this work, the focus lies on intercarpal instability (ICI), of which the most common is dorsal intercalated segmental instability (DISI), and midcarpal instability (MCI). Several clinical measurements are used to assess these instabilities. For MCI, the capitolunate angle is typically the most important metric. For DISI, the scapholunate angle is most often used [24]. These angles are most often measured on lateral x-ray images and are shown in Fig. 2.1. Section 3.3 will go further into how these angles are measured.

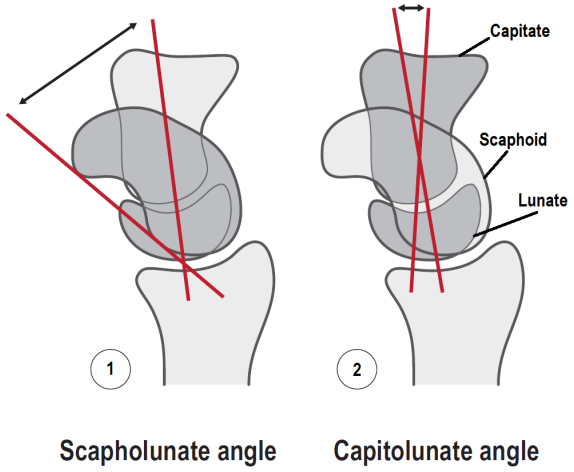

Figure 2.1: Bone angles of interest. Lateral view of the wrist. 1) Scapholunate angle 2) Capitolunate angle. Edited from [24].

2.3. Research questions and goal

The goal of this thesis is to develop a motorized motion guidance device for the wrist to be used in combination with a 4D CT scanner and test its performance experimentally. This device should be able to perform standardized movements in the most important motion planes for the wrist. As the images are made by a CT scanner, a CT protocol had to be set up. Several protocols exist in the literature [12, 25] and it was decided to vary two variables (motion speed and radiation dosage in the form of tube current) to find their effect on image quality. The rationale behind these variables will be explained in chapter 3.2.

Taking the above into account, the research question which arises from this goal is as follows:

Can a designed motorized motion guidance device for the wrist yield reliable 4D CT images to be used in kinematic analysis?

The following subquestions arise from this question:

1. **How should a motion guidance device with the goal of yielding reliable 4D CT images be designed?**
2. **How can the 4D CT scans acquired with this device best be performed?**
3. **How can the reliability of the retrieved 4D CT images of a wrist in motion be tested?**

The case of dynamic wrist instability is used to answer these questions and evaluate the performance of the device. This means that the focus lies on the measurement of the angles of the scaphoid, lunate and capitate, which are the most important bone angles to take into account when diagnosing carpal instability.

In this work, several terms are used to describe the motion guidance device. Motion rig, motion device, motion guidance device, wrist holder, and wrist device can all be used interchangeably. Furthermore, when reading about wrist kinematics, the focus lies on carpal kinematics. These terms will also be used interchangeably.

2.4. Outline

The following chapters will all roughly have the same structure and will be divided into three parts, each of them focusing on one of the subquestions stated above. The first part will describe the design and design process of the motion device. The second part will describe the experiments and scanning procedure. The third part will describe the post-processing that was done after the retrieval of the data.

In chapter 3, the details of the methodology will be described. Chapter 4 will describe the results from the same sections found in the Methods. In chapter 5, the results of the three subsections will be interpreted and discussed. Improvements and insights will be shared, and the limitations of this work will be considered. Chapter 6 will be the concluding chapter for the whole thesis.

3
Methods

In this chapter, the methodology of the project will be gone into. The design criteria and process are described in section 3.1. After this design process, a cadaveric experiment was performed with 4D CT scans, of which the details can be found in section 3.2. The scans from this experiment were then collected and analysed. Measurements were made and statistical analysis followed. This process is described in section 3.3.

3.1. Design

3.1.1. Design criteria

The main goal for the design is to develop a motion guidance device which is able to move the wrist in a CT scanner. The images collected from this are valuable during the diagnosis of both intercarpal and midcarpal wrist instability. The most important metrics for this diagnosis are the scapholunate angle and capitolunate angle during both flexion-extension (FE) and radial-ulnar deviation (RUD) of the wrist. The device, therefore, has to be able to perform standardized and smooth motions of both FE and RUD of the wrist. In this thesis, the device is meant to be used in an experimental setting with cadaveric specimens. In the future, live participants and patients might also use the device. This should be kept in mind in the design process. Earlier testing on specimens proposed an average needed torque of around 2 Nm for FE for cadaveric experiments. Based on a surgeon's input, and the fact that overcoming gravity plays a smaller role in RUD, it was assumed that the torque needed for RUD would not be larger than this.

Because of the use of the device inside a CT-scanner environment, several limitations are present in the choice and placement of materials and electronic parts. Because metals and other non-radiolucent materials leave artefacts on the scans, the scanning area should not contain any non-radiolucent materials. Additionally, operators should not have to be close to the device while operating it, because of the radiation present during a CT scan.

The device is meant to be used with a wide range of use cases, both in research and clinical settings. To this end, it should be usable with cadaveric specimens as well as patients. Because hand sizes differ widely, it should be able to accommodate different hands. As a reference measure, surgical gloves were used to represent different hand sizes. Glove sizes 6 to 9 were measured from the most proximal part of the wrist to the approximate middle point of the palm. This distance was used as a reference for the distance between the rotation axes and the part where the hand should hold the bar.

For easy prototyping and reparation or replacement of broken parts, the device should be modular. Modularity also facilitates improvements further down the line and in future projects, without the need for a full redesign. Furthermore, it improves transport, storage, and cleaning possibilities. Because the device is being used by patients and/or specimens, cleaning is necessary between measurements.

The above considerations have been summarized in the following list, where both requirements and wishes of medical specialists are included:

- The device must be able to perform the following motions, both motorized and non-motorized:
  - FE from 40° extension to 40° flexion

  - RUD from 30° ulnar to 15° radial deviation
- The drive system must have the following specifications:
  - A minimum torque at low speed of 2 Nm for both FE and RUD
- The device must be able to be used in a CT-scanner environment:
  - no metals or other non-radiolucent materials inside the scanning area
  - the operator does not need to be near the device during the movements.
- The device must be able to be used in different cases:
  - both patients and specimens
  - hands ranging from glove size 6 to 9
  - both right and left hands
- The device must be modular and easily adjustable
- The device must be easily cleanable

3.1.2. Preliminary design

Earlier versions of a motion device were already worked on by students of both the TU Delft and Haagse Hogeschool. This version of the device is shown in fig. 3.1. However, there were no technical drawings available, and the device had several points to be improved on. This design provided a good basis on which a more elaborate and complete design could be built. The design consisted of a main base and plateau on which an arm can be put (fig. 3.1A). This base is connected to a set of parts which can move around, providing motion to the wrist (fig. 3.1D).

Although this device was a good starting point, several issues were present. First, the device had several structural issues. It contained several metal bolts in the scanning area because nylon bolts in those places had not proven strong enough (Fig. 3.1D). Furthermore, some of these bolted connections would loosen after a few uses. The base of the device and the part where the hand is put in were only connected by two bolts on the same axis, allowing for unwanted rotations (fig. 3.1E). Also, without the connected locomotive drive, the base would fall over due to the weight of the moving arm.

Secondly, the drive system which was chosen was not structurally connected to the motion device, resulting in relative motion between these two parts (fig. 3.1C). Furthermore, the locomotive drive allows for dead points and blockages in the drive, especially without proper bearing. The device also lacked the ability to perform motorized RUD. The whole system ran on a 5 V power supply with the motor being powered through the microcontroller, and the chosen stepper motor was not strong enough to move the system.

Lastly, the device was largely glued together, lacking any kind of modularity or adaptability. Due to these shortcomings, it was decided to entirely redesign the existing motion rig, taking into account the lessons learned from previous versions.

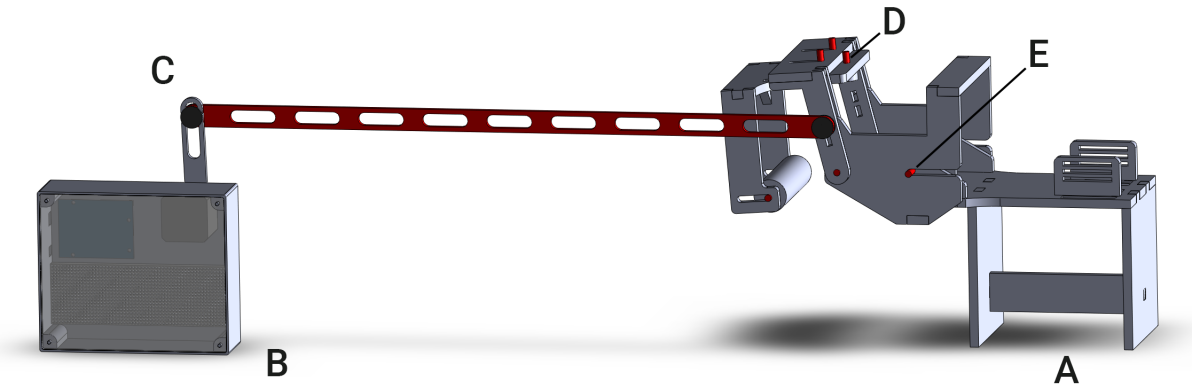

Figure 3.1: Device as presented at the start of this project. A) Base with plateau to lay arm on. B) Electronics housing. C) Locomotive drive. D) Moving arm with metal bolts. E) Single axis which connects the base to the moving parts.

3.1.3. Design process and manufacturing

The design process existed of several steps. First, a list of design criteria was established in close collaboration with a hand and wrist surgeon, where the goal of standardization of motion was central. Second, the existing motion rig was analyzed for its defects based on these goals. Third, the device was re-designed. Fourth, in an iterative prototyping process, parts were manufactured and introduced to the device. New additions were tested for their fit and use, after which they were adjusted and remanufactured if necessary.

All technical drawings were made using SOLIDWORKS® CAD software *(version 2021 SP5.0, Education Edition, Dassault Systèmes SolidWorks Corp, Waltham, Massachusetts, USA)*. PMMA parts were laser cut at the student workshop of the Faculty of Mechanical, Maritime and Materials Engineering (3mE) of the TU Delft. Some additional parts were 3D printed with a modified Creality Ender 3 printer *(Creality, Shenzhen, China)* and eSun PLA+ filament *(Shenzhen Esun Industrial Co., Ltd., Shenzhen, China)*. In designing the PMMA connections, a test tool was designed to evaluate the tolerances of the laser-cut PMMA as seen in fig. 3.2.

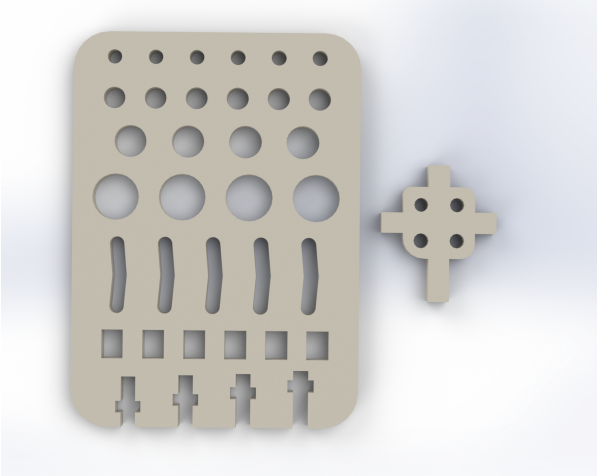

Figure 3.2: Evaluation tool used to evaluate the tolerances of the laser-cut PMMA. All holes are of different sizes.

3.2. Experiment

To evaluate the performance of the newly designed tool, an experiment with three cadavers was established. Varying the speed of the guidance device and radiation dosage, multiple 4D CT scans per specimen were acquired. Speed and radiation dosage were varied to research their effects on image quality.

3.2.1. Variables and scan protocol

Faster movement of the guidance device can cause motion artefacts [26]. Therefore, the motion speed of the specimens was considered as one of the variables.

Quick motions could result in more motion artefacts, and thus it was theorized that motion speed could have an effect on the reliability of the final images. Motion speed was defined as either static, slow or fast. Static is defined as a non-moving wrist. Slow is defined as a rotation speed of the motor of 15 steps per second. As later specified in chapter 4.1, the motor has a stepsize of 1.8°, so this results in an angular velocity of 27° per second, or $\frac{3\pi}{20}s^{-1}$. Fast is defined as a motor rotation speed of 50 steps per second, which is 90° per second or $\frac{\pi}{2}s^{-1}$. These angular velocities were selected following velocity values reported in literature [12, 27].

As for the radiation dosage, this was varied by changing the tube current. This has a direct effect on the effective dosage. As the lower value, 15 mA was chosen. This is a significantly lower value than what is commonly used and was chosen following the work of Dobbe et al., who have done a study towards evaluating 4D CT-protocols [12]. As the normal value, a tube current of 80 mA, which is the most commonly used value for this kind of scan [7, 12], as discussed with the radiotechnician. While the yearly limit of radiation dosage is about 1.0 mSv and both of the values in table 3.1 is significantly

Table 3.1: Scan parameters used in the experiments

Variable	Value
Tube Current (low and high)	15 or 80 mA
Tube Potential	80 kV
Scanning range	140.0 mm
Display Field of View (DFoV)	120.0 mm
Effective mAs	28 mAs
Total scan time	12.75 s
Reconstruction time	0.25 s
Effective Dosage (low and high)	0.08 mSv or 0.015 mSv

Effective dosage is DLP multiplied by the conversion factor for hand/wrist/ankle (0.0002)

lower than that, it is interesting to investigate what kind of effect an even lower value has on image reliability.

Each scan took 12.75 seconds with a reconstruction time of 0.25s. This resulted in a total of 51 reconstructed volumes per scan. Table 3.1 was used as a scan protocol and was based on typical values used in CT scanning for the wrist in close collaboration with a radiotechnician from the Reinier de Graaf Hospital in Delft.

3.2.2. Specimens

Three cadaveric arms were used in this study, with the approval of the medical ethical committee of the Reinier Haga Orthopedic Centre (RHOC). This amount was chosen based on both similar studies done in the past [6, 28, 29], and the practical availability of specimens. The specimens were to be amputated below the shoulder but above the elbow, and should not have a history of wrist injury or other pathologies.

3.2.3. Experimental setup

For the 4D CT scans, a Toshiba Aquilion One CT scanner *(Canon Medical Systems Corporation, Otawara, Tochigi, Japan)* was used. The motion device was securely put on a wooden board with tie wraps through holes in the base of the device (fig. 4.2)C, which was placed on the CT table. The specimens were secured in the device by Velcro straps. The weight and friction of the hands themselves on the handle bar proved enough to facilitate motion, it was not deemed necessary to attach the hands to the device more securely. Fig. 3.3 shows a specimen in the motion device.

Per specimen, 6 scans were made, as displayed in table 3.2. The first scan was a 4D scan made of a non-moving (static) wrist with a tube current of 15 mA. To isolate the radiation dosage variable, no movement was used in this scan. The second scan was also a scan of a static wrist, but this time with a tube current of 80 mA. The third and fourth scans were made of a slow-moving wrist with a default tube current of 80 mA. They performed movements from extension to flexion and from radial to ulnar deviation, respectively. The fifth and sixth scans were made of a fast-moving wrist with the default tube current of 80 mA. They performed the same motions as the third and fourth scans, moving from extension to flexion and from radial to ulnar deviation, respectively. The experimental protocol is included in Appendix A. The angle of the capitate relative to the radius was used to define wrist movement in the sagittal plane and the coronal plane to measure FE and RUD respectively [5, 30, 31].

3.3. Post-processing of 4D CT scans

The data that was retrieved from the CT scanner consisted of a series of DICOM images, each representing a single frame of a 4DCT scan. First, the DICOM images were imported, organized and viewed in 3D Slicer *(Version 5.0.3)* [32, 33]. Initially, the scans existed of the same amount of frames, so only the timeframe where the wrist was moving had to be selected. The frames where the wrist was moving were exported and saved as a sequence in 3D slicer, including one frame before and after the movement as a t_0 and t_{end}.

In clinical usage, SL and CL angles are evaluated using lateral views [24]. Therefore, using both a 3D and a lateral view in 3D slicer, a lateral slice was selected per frame for the lunate, the scaphoid,

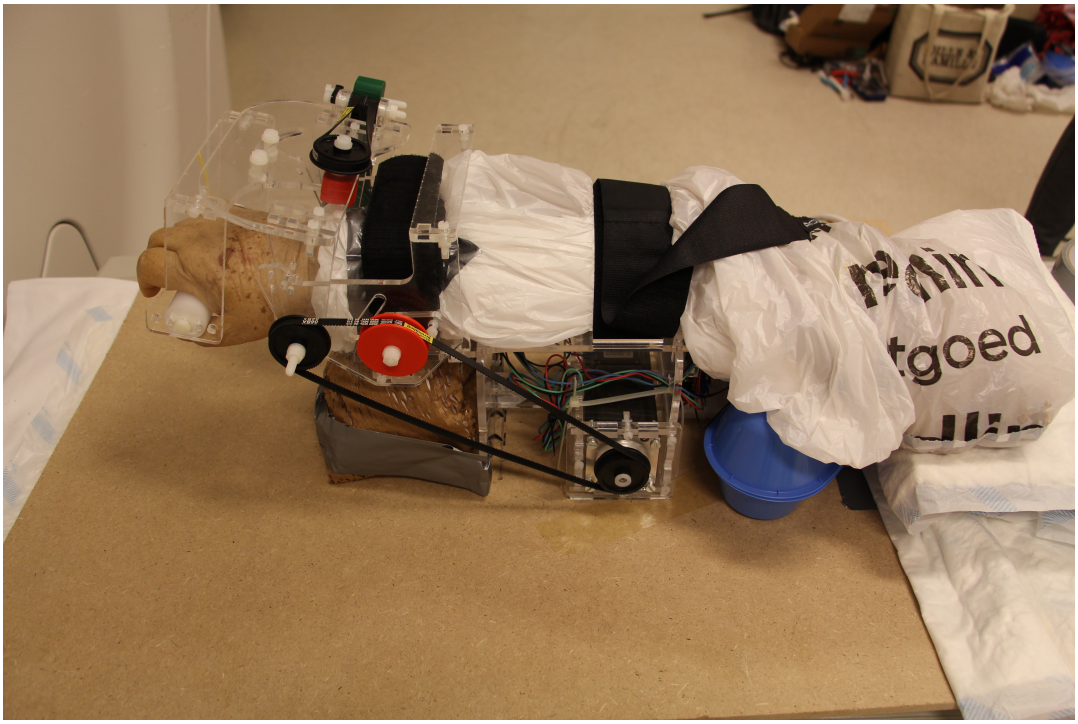

Figure 3.3: Cadaveric sample secured in the motion device

Table 3.2: Different scans made per specimen.

Scan number	Tube Current (mA)	Movement	Speed
1	15	Static	0
2	80	Static	0
3	80	FE	Slow, 27°/s
4	80	RUD	Slow, 27°/s
5	80	FE	Fast, 90°/s
6	80	RUD	Fast, 90°/s

FE: Flexion-Extension. RUD: Radioulnar Deviation

and the capitate to measure the individual bone angles. To select this slice, a line was drawn in 3D view for all three bones of interest (fig. 3.4). The 2D slice where this line was most visible was selected (fig. 3.5). This slice was converted to a JPG image to be analysed later.

The slice for the lunate was selected by drawing a line between the two most distal points of the lunate. The Scaphoid slice was selected by drawing a line in 3D view between the most outer point on the proximal surface and the middle point of the distal convex surface. The slice for the capitate was selected by drawing a line between the most proximal part of the proximal convex surface and the middle point of the distal concave surface.

The result of this process is a total of three slices per frame per scan: One for the lunate, one for the scaphoid and one for the capitate. An example of this is shown in fig. 3.5. In each of these images, the bone angle of the bone of interest was measured twice by both the author and a hand and wrist surgeon. The images were randomized before measurement. The measurement was done in ImageJ, *(version 1.53, Wayne Rasband and contributors, National Institutes of Health, USA)*. The angle was measured by drawing a line according to fig. 3.6. Because there were a lot of images to be measured, a custom macro was written to make this measurement process as easy as possible. This macro can be found in appendix B. After drawing the line representing the bone angle of interest, this macro would calculate the angle between the drawn line and a neutral line. This neutral line is the same between all images and is a line of 0°. It would then save the image, and open the next image. After measuring the individual bone angles, the SL angle was calculated by deducting the scaphoid angle from the lunate angle. The CL angle was calculated by deducting the lunate angle from the capitate angle.

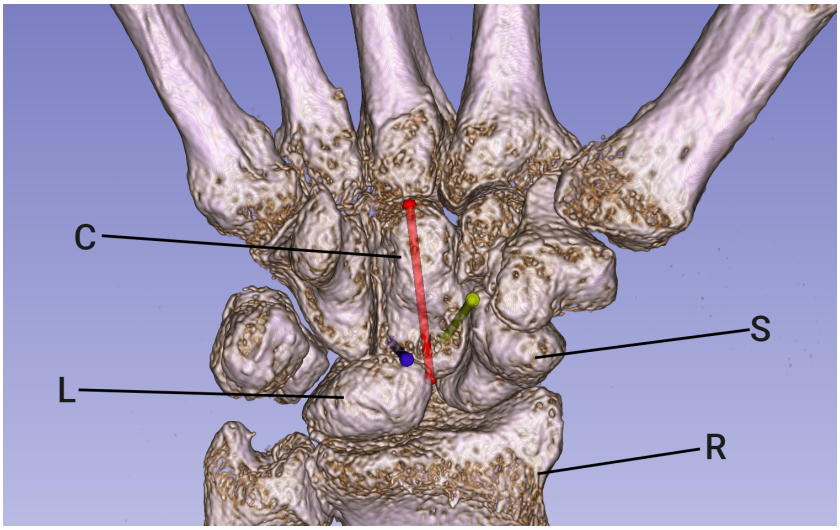

(a) Volar view

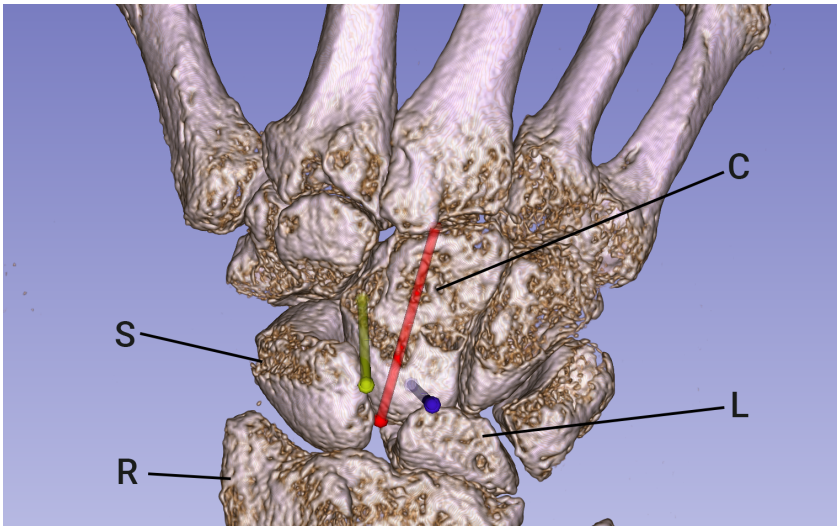

(b) Dorsal view

Figure 3.4: Screenshots of lines drawn in slicer in 3D view for lunate (blue), scaphoid (green) and capitate (red). S, scaphoid. R, radius. L, lunate. C, capitate.

For statistical analysis, data was gathered and organized in Microsoft Excel *(Version 2210, Microsoft, Albuquerque, New Mexico, USA)*, and analysed in IBM SPSS Statistics 28 *(Version 28.0.1.1 (15), IBM, Armonk, New York, USA)*. For the statistical analysis, the Intraclass Correlation Coefficient (ICC) was used as a metric for the reliability of the measurements. The ICC was used to calculate both intra-observer and inter-observer reliability, which were compared for radiation dosage and movement speed to provide a metric of how reliable images acquired with the help of the device are for measuring the bone angles of interest. ICC types were determined based on Koo et al. [34]. For intra-observer reliability, a two-way mixed-effects model based on absolute agreement with single measurements was used. For inter-observer reliability, a two-way random-effects model was used, based on absolute agreement using the mean of multiple measurements.

(a) 2D slice with good view of the drawn lunate line in 3D

(b) 2D slice with good view of the drawn scaphoid line in 3D

(c) 2D slice with good view of the drawn capitate line in 3D

Figure 3.5: Screenshots of 2D slices with good views of drawn lines in 3D. Line thickness is exaggerated for visibility

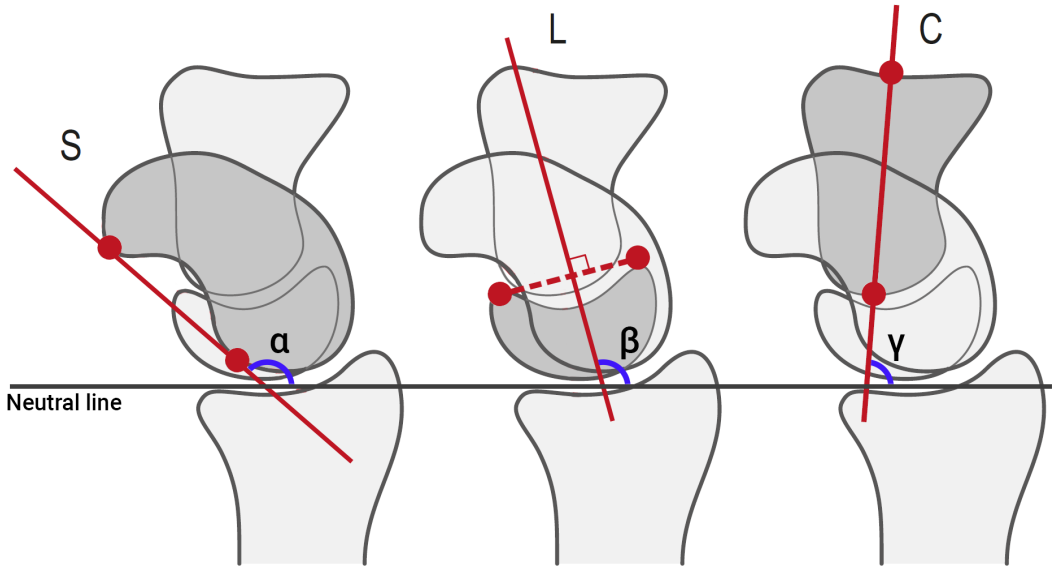

Figure 3.6: How the angles were measured. (S) The scaphoid axis is constructed by drawing a line connecting the two palmar convexities of the scaphoid. (L) The lunate axis is measured perpendicular to the line which connects the two distal horns of the lunate. (C) The capitate axis is drawn through the centre of both the proximal and distal surfaces. Edited from [24]

4

Results

After iterating and prototyping several times, the final design was evaluated and completely manufactured. The results of this process are reported in section 4.1. This final design was then used in an experiment with a 4D CT scanner, of which the data and observations during the experiment are reported in section 4.2. The measurements that were done afterwards are reported in section 4.3.

4.1. Design

4.1.1. Overview

The process to design the motion guidance device took several iterations and prototypes. The final version is shown in fig. 4.2. The device consists mostly of laser-cut PMMA parts, ranging in thickness from 6 mm to 8 mm. The parts shown in fig. 4.2 are opaque to provide a clearer image, however the real parts are transparent, as seen in fig. 4.5. The transparent material makes cleaning easier because material inside grooves can be seen too, but it also provides the operator with a clearer view of the hand and arm. To provide for modularity, the laser-cut parts are connected by an interlocking system which is tightened by nylon bolts and nuts, as shown in fig. 4.1. This mechanism provides a tight connection while still being able to be loosened and replaced. The only metallic parts in the design are the stepper motors and their wiring, the Arduino microcontroller which can't be seen in fig. 4.2 because it is on the back of the device, and the bolts which hold the stepper motors in place. These are all outside the scanning range, and will not provide artefacts on the scans.

The device consists of a plateau to rest an arm on, perforated with slots to allow for the attachment of Velcro straps. These straps make sure the arm can be mounted securely on the platform and will not move during scanning (fig. 4.2A). The hand will hold or be attached to a bar connected to a swivelling arm (fig. 4.2E), which is connected to the main carriage (fig. 4.2G). These two parts will make the hand move. The rotation axes of the wrist can be lined up with the rotation axes of the device by moving the bar to another set of holes in the sides of the handle. These holes have been spaced corresponding to wrist position in glove sizes 6 to 9, or XS to L. The motions are provided by two stepper motors, which are housed securely in the back of the device (fig. 4.2B). There are small ventilation holes to provide for enough cooling. These motors drive two timing belt systems, one for FE (fig. 4.2D) and one for RUD (fig. 4.2F). The neutral stance of the moving parts of the device can be adjusted by a small bolt shown in fig. 4.3B. Fig. 4.2 shows holes to fix the device to a wooden plate.

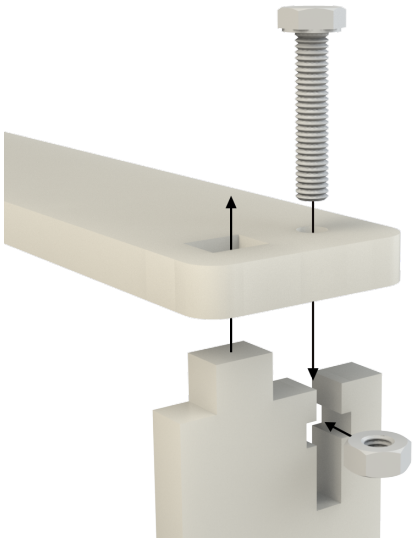

Figure 4.1: Exploded view of a rendered bolt connection

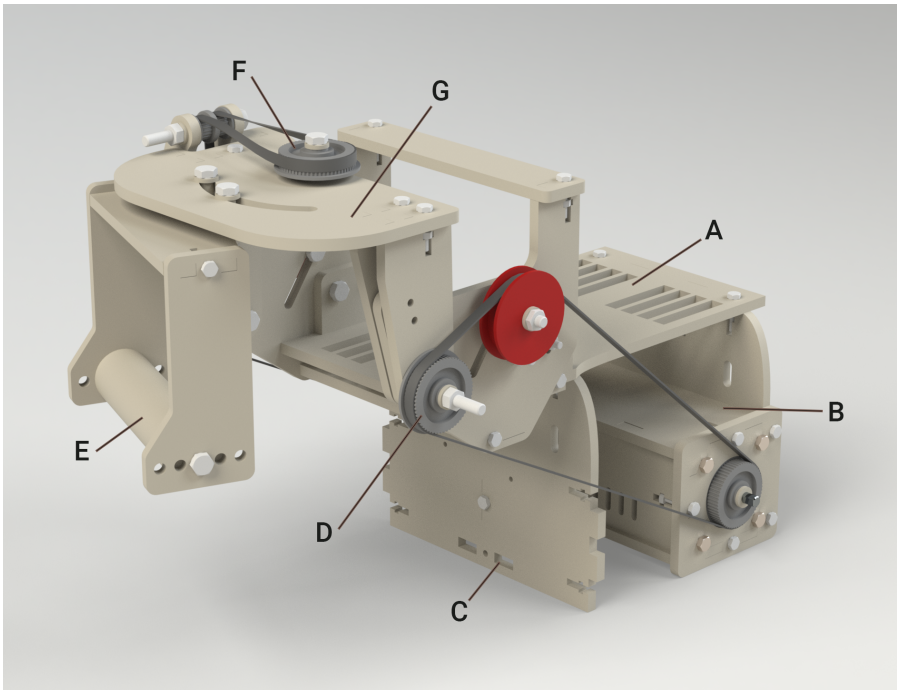

Figure 4.2: Render of the motion guidance device. A) Plateau for arm to rest on with slots for Velcro straps to pass through. B) Stepper motor housing with two bipolar NEMA 23 stepper motors. C) Holes for attaching the device to a wooden board. D) Timing belt array for flexion/extension. E) Swivelling arm with bar to hold or attach hand to. This part will swivel left and right (RUD) F) Timing belt array for ulnar and radial deviation. G) Main carriage. This part will move forward and backward (FE).

4.1.2. Drive system

The motions are driven by two stepper motors. These motors drive two timing belts, which are 6 mm wide RS Pro MXL rubber belts with a 2.032 mm pitch. The timing belts are accompanied by several pulleys, which are flanged RS PRO glass-filled PC pulleys with either 20 or 60 teeth. The belt is tensioned by an additional 3D-printed pulley in an adjustable slot, as shown in fig. 4.3C. The bearings that are used are plastic polyamide slide bearings.

The left timing belt drives the forward and backwards rotation of the main carriage of the device, which results in a FE motion of the wrist (fig. 4.3). The gear shown in fig. 4.3D protrudes into the main carriage, form-fitting into the leftmost arm of the carriage. The motion can be locked both by the motor and by putting a small rod in the hole on the left side of the carriage, just above the large pulley (fig. 4.3D). FE is possible from 80° extension to 80° flexion.

RUD is guided by a swiveling arm, driven by two timing belts in series, as shown in fig. 4.4. The first belt runs along the right side of the device, like the FE belt. However, because the axis of RUD motion is perpendicular to the FE axis, the drive has to be angled 90°. This is done by twisting a second timing belt over a set of two small gears. These two belts are connected by a double gear (fig. 4.4C). Although unusual, such a timing belt setup is functional and allows for out-of-plane rotation, which is very useful in this case. In designing this angled drive, considerations from a handbook for timing belts were taken into account [35]. Two bolts in the top plate guide the handle through an arched slot, which allows RUD from -34° to 34°, making it suitable for both left and right hands.

4.1.3. Electronics

Fig. 4.5 shows the device and all its electronics connected in an experimental setting. The two stepper motors (fig. 4.5D) are bipolar, 24VDC, 1.4 A/phase motors with a NEMA 23 dimension profile. They offer a holding torque of 2.08 Nm. They are powered by a Mean Well 125 W dual output power supply (fig. 4.5A). This power supply has both a 12 V and 24 V output with a rated current of 3.7 A. The motors are controlled by an Arduino UNO R3 microcontroller which is connected to two individual TI DRV8825 stepper motor drivers, which are current limited to 1.4 A. This was done following equation 4.1 [36]. As the current limit of the stepper motors is 1.4A, V_{ref} was set to 0.7 V.

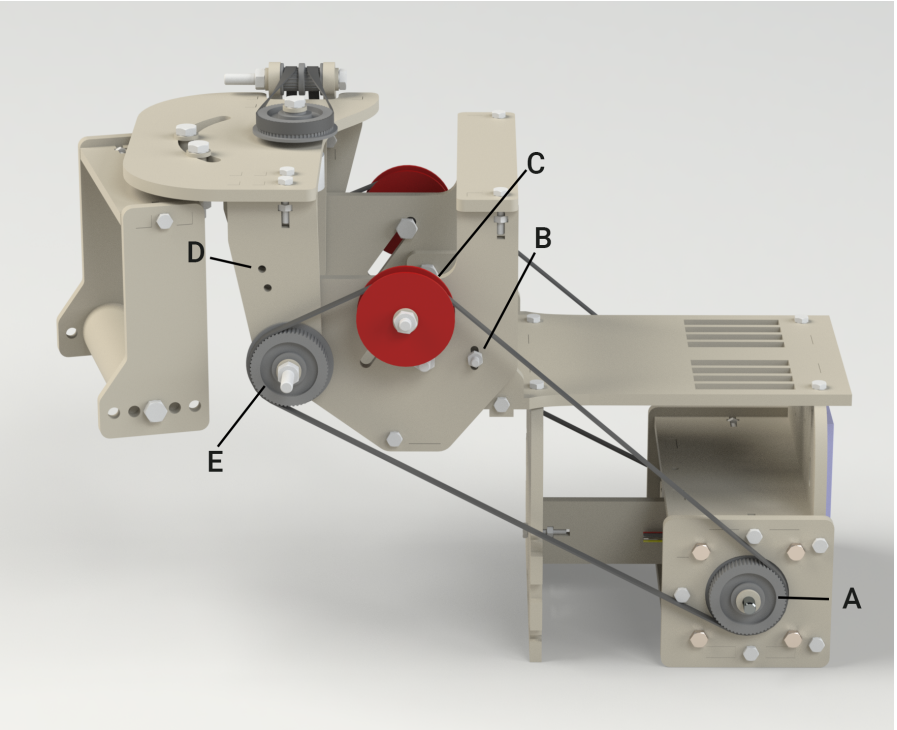

Figure 4.3: FE motion system. A) Stepper motor for FE. B) Bolt to adjust standard rotational position. C) 3D printed belt tensioner. D) Holes to lock FE motion by means of a bolt through the arms. D) Gear which conveys motion to the swivelling arm.

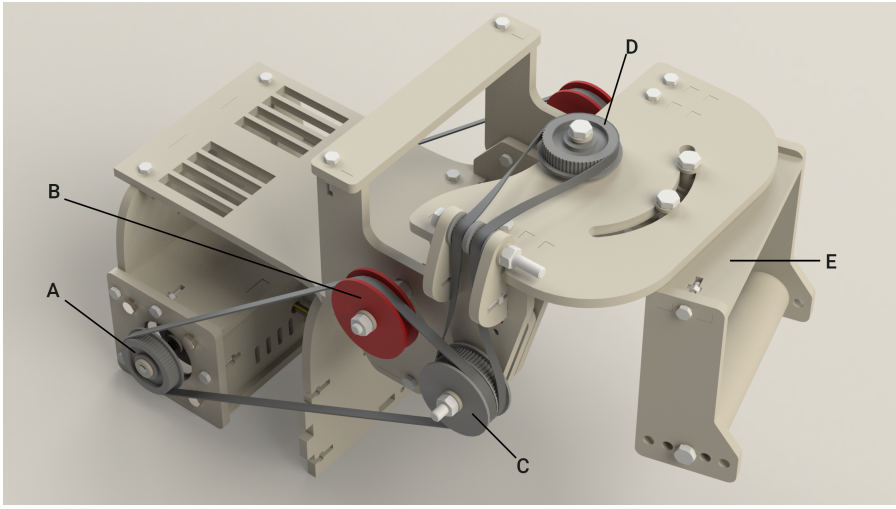

Figure 4.4: RUD motion system. A) Stepper motor for RUD. B) Belt tensioner. C) Double gear which translates motion to the next belt. D) Gear which conveys motion to the swivelling arm. E) Swivelling arm.

$$V_{ref} = \frac{Current\ limit}{2} \tag{4.1}$$

The Arduino microcontroller is powered by the 12V output of the power supply. The motors are powered by the 24V output. To connect all the electronics a screw terminal shield was used, on which several connections were soldered (fig. 4.5C). The Arduino microcontroller can be activated with three buttons (fig. 4.5B), each putting the device in a different state. These states are a resting state, FE, and RUD. Once pressed, the device will wait a defined amount of time, so that the operator can go out of the room. The movement will then take place.

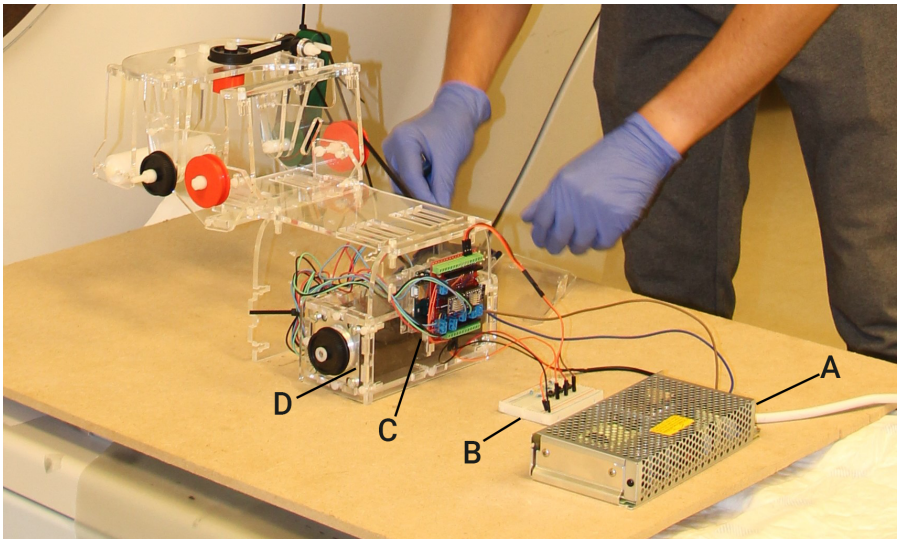

Figure 4.5: Overview of the device and electronics in experimental setting. A) Power supply. B) Buttons to select movement mode. C) Arduino and screw terminal shield. D) Stepper motors.

4.2. Experiment

The movements that were performed during the scans differed per specimen used, mainly because of specimen stiffness. The specimens were each forced to move a specified amount in FE or URD. This movement entailed 72° for both FE and URD. Movement stopped when the device reached this amount of rotation or when the specimens proved too stiff for the device to move further. Mainly in the third specimen, this was caused by a lack of rigidity of the device, which will be discussed below and in section 5.1. Table 4.1 summarizes the difference between specimens well. During the experiments, it was found that the second and third samples were operated on before. In the case of the second specimen, this did not result in any extra stiffness or other difficulties. It might even have caused the generally larger range of motion when compared to the other two. The third sample however was visibly and noticeably affected. It had large scars and significantly impacted anatomy of the carpal bones in the form of cysts. Clearly visible in this table, the third specimen was much stiffer than the others. While the hand in its entirety moved during the scans, relative motion between carpal bones and the radius was minimal, only moving a few degrees at most. Because of the minimal amount of movement this sample offered, it was chosen to not include its data in further analysis.

In fig. 4.6, an example of the measurements of one scan is shown. In this example, the measurements for the lunate (Fig. 4.6a), scaphoid (Fig. 4.6b) and capitate (Fig. 4.6c) angles are shown for the first and second specimen. The movement performed was FE under low speed. The total movement included 11 volumes for the first specimen and 12 for the second. The resulting SL and CL angles are shown in Fig. 4.7.

During the experiments, several issues were noted, which will shortly be described here. First, the stiffness of the PMMA parts and axes in the structure was not always sufficient, with the device bending slightly when put under load of both the weight of a specimen and the provided torque of the motors. This resulted in the gears being pulled towards each other, loosening the belts, and therefore decreasing the torque the motor could deliver effectively.

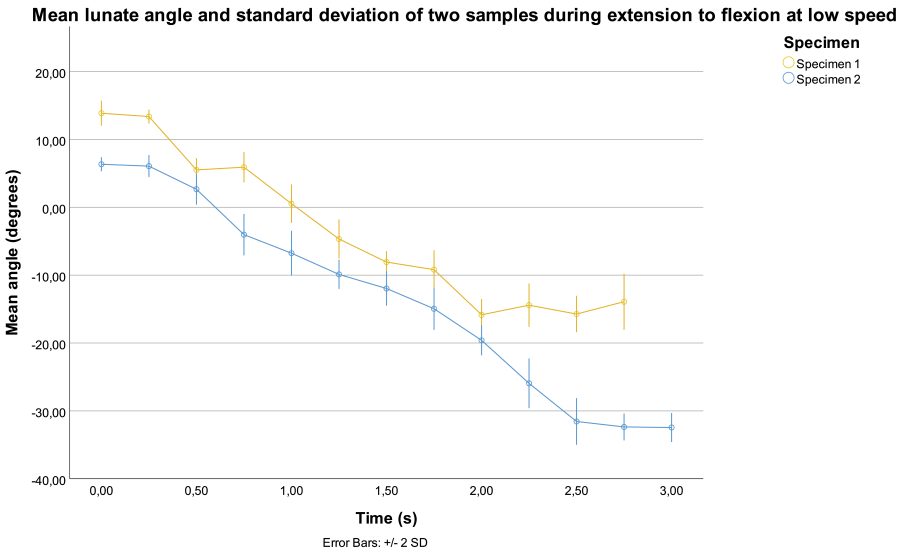

(a) Lunate angle

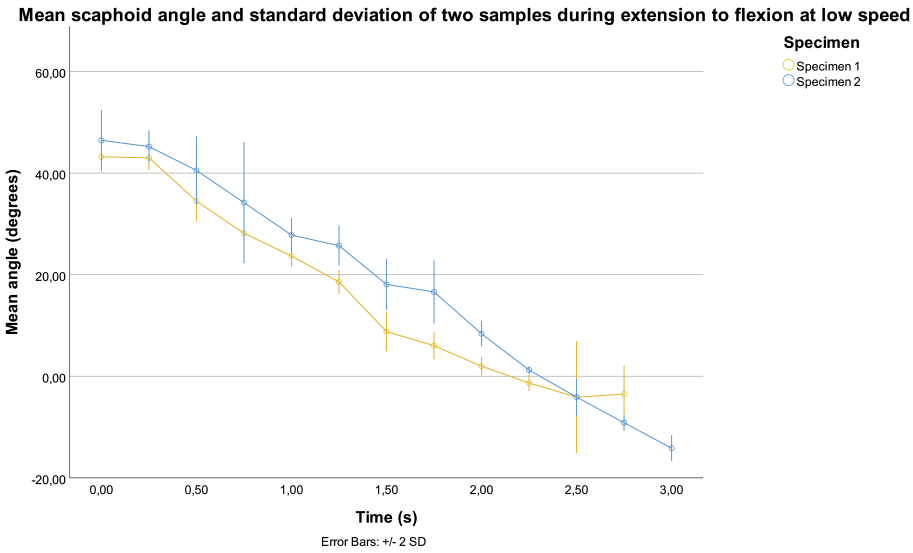

(b) Scaphoid angle

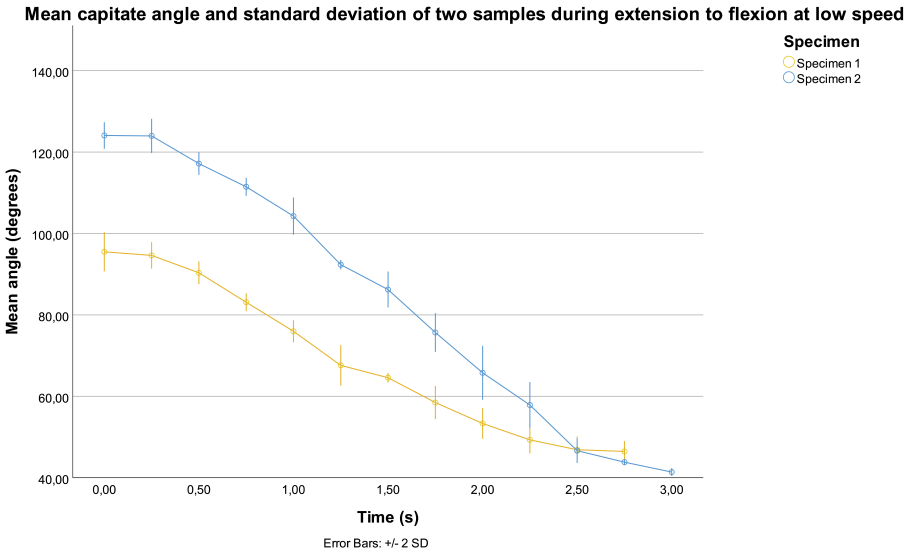

(c) Capitate angle

Figure 4.6: Measured bone angles per time frame during extension to flexion. Low speed.

Table 4.1: Average movements per sample

Movement	Specimen 1	Specimen 2	Specimen 3
Extension to flexion (slow)	10° to -38°	32° to -43°	12° to 10°
Extension to flexion (fast)	10° to -38°	34° to -42°	15° to 11°
Radial to ulnar deviation (slow)	10° to -10°	30° to -3°	18° to 17°
Radial to ulnar deviation (fast)	10° to -12°	30° to -1°	18° to 17°

All angles are relative to the radius axis. Extension angle is positive, flexion negative. Radial deviation angle is positive, ulnar deviation negative.

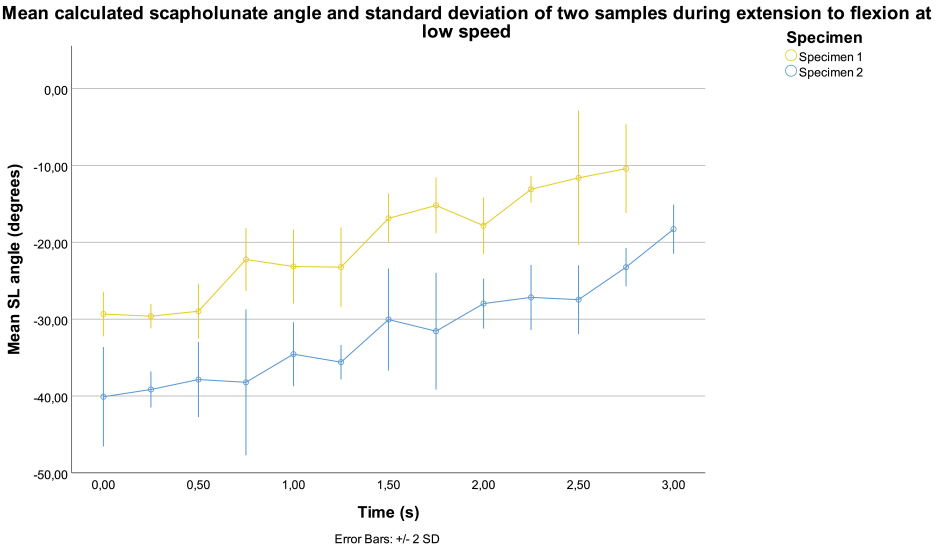

(a) SL angle

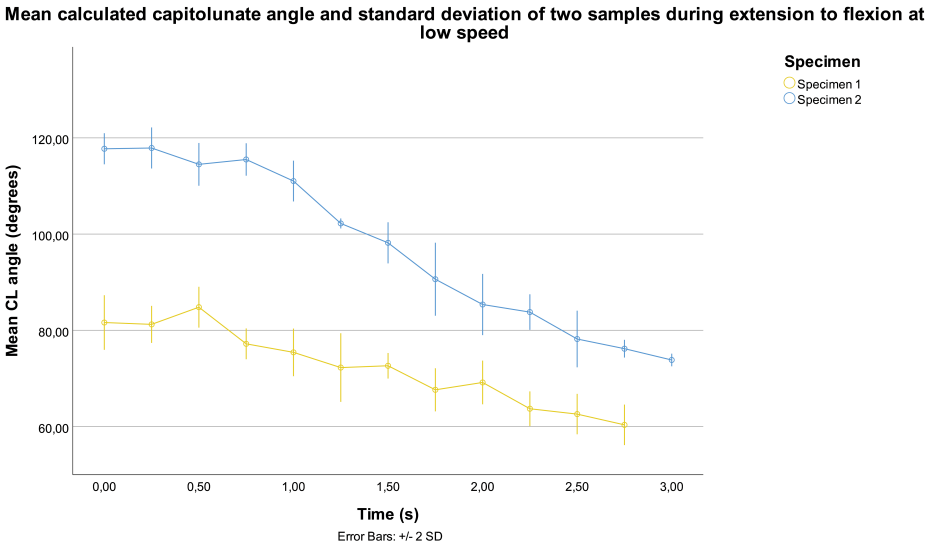

(b) CL angle

Figure 4.7: Calculated scapholunate and capitolunate angle during extension to flexion. Low speed, specimen 2

Second, the RUD movement was not running optimally. It is driven by a 3D-printed double gear made of PLA, shown in fig. 4.4C, which wears quite quickly, causing the belt to slip. Furthermore, the belt comes together at the point of the 90° angle, reducing the possible torque which can be transferred. Lastly, there should be an easy way to lock RUD motion in place. During the experiments, this had to be done with a tie wrap, which is inconvenient.

4.3. Post-processing

Table 4.2 shows all calculated ICCs for intra- and interobserver agreement for the different measured bone angles in every experiment, and the resulting calculated SLA and CLA. Since every measurement was performed twice by each rater, an intra-observer agreement can be calculated. These first and second measurements are used on their own to calculate inter-observer agreement for both of these measurements.

What stands out is the fact that most of the presented values in table 4.2a and 4.2b are above 0.75 and even 0.9, indicating good and excellent reliability of the measurements respectively [34]. It is noted however that some scaphoid measurements offer significantly lower ICC values. Especially the low dosage measurements provide low ICC, falling below 0.6 in the case of the intra-observer agreement of the first rater and even below 0.2 in the case of the intra-observer agreement of the second rater and the inter-observer agreement of the first measurement. To examine this finding further, a third observer was asked to measure some of the scaphoid scans with a low ICC (< 0.75) or consistently low lower bounds of the 95% confidence interval (<0.7). The scans that were measured again were the scans of the scaphoid with no movement and RUD movement since these presented the lowest ICC or largest 95% confidence interval. The third observer was a resident orthopaedic surgeon (Bas Aarts) at the RHOC. The recalculated ICC values including the third observer have been summarized in table 4.3. A few things stand out here. First of all, the ICCs for no movement and low dosage are also very low for the third observer. Furthermore, the ICC for intra-observer agreement for high-speed RUD movement is very low in comparison with the values in table 4.2 (0.490 compared to 0.900 and 0.732). Lastly, it seems that the inter-observer agreement for the first measurement ends up lower than the agreement for the second measurement, which was not necessarily the case with the first two raters.

Table 4.2: Intraclass correlation and 95% confidence interval for intra- and inter-observer agreement of measured bone angles and resulting scapholunate and capitolunate angles

(a) Intraclass correlation for intra- and inter-observer agreement of measured bone angles

Experiment	Bone measured	Intra-observer 1	95% Confidence Interval		Intra-observer 2	95% Confidence Interval		Inter-observer 1	95% Confidence Interval		Inter-observer 2	95% Confidence Interval	
		ICC	Lower bound	Upper bound	ICC	Lower bound	Upper bound	ICC	Lower bound	Upper bound	ICC	lower bound	Upper bound
No movement, low dosage	Lunate	0,970	0,887	0,992	0,981	0,924	0,995	0,987	0,949	0,997	0,972	0,892	0,993
	Scaphoid	**0,523**	**-0,742**	0,879	**0,167**	**-2,761**	0,798	**0,128**	**-3,665**	0,796	0,780	0,119	0,945
	Capitate	0,989	0,635	0,998	0,974	0,894	0,994	0,965	0,663	0,993	0,970	0,333	0,995
No movement, high dosage	Lunate	0,988	0,955	0,997	0,970	0,887	0,993	0,971	0,845	0,993	0,974	0,897	0,994
	Scaphoid	0,946	0,723	0,987	0,932	0,743	0,983	0,903	0,626	0,976	0,905	0,608	0,977
	Capitate	0,992	0,953	0,998	0,979	0,844	0,995	0,977	0,882	0,994	0,964	0,428	0,993
FE, low speed	Lunate	0,998	0,996	0,999	0,995	0,989	0,998	0,996	0,990	0,998	0,994	0,988	0,998
	Scaphoid	0,994	0,987	0,998	0,990	0,978	0,996	0,987	0,970	0,994	0,995	0,988	0,998
	Capitate	0,998	0,996	0,999	0,997	0,993	0,999	0,997	0,994	0,999	0,998	0,993	0,999
RUD, low speed	Lunate	0,995	0,988	0,998	0,979	0,953	0,991	0,977	0,945	0,990	0,986	0,936	0,995
	Scaphoid	0,935	0,855	0,971	0,835	0,631	0,926	0,911	0,742	0,964	0,874	0,618	0,950
	Capitate	0,997	0,993	0,999	0,987	0,970	0,994	0,988	0,973	0,995	0,991	0,975	0,996
FE, high speed	Lunate	0,998	0,992	1,000	0,994	0,981	0,998	0,992	0,934	0,998	0,989	0,582	0,998
	Scaphoid	0,994	0,981	0,998	0,998	0,994	0,999	0,998	0,993	0,999	0,996	0,985	0,999
	Capitate	0,998	0,993	0,999	0,998	0,993	0,999	0,994	0,980	0,998	0,988	0,959	0,996
RUD, high speed	Lunate	0,979	0,940	0,993	0,982	0,935	0,994	0,983	0,952	0,994	0,972	0,498	0,994
	Scaphoid	0,900	0,700	0,966	**0,732**	0,208	0,907	0,832	0,535	0,941	0,904	0,730	0,966
	Capitate	0,992	0,978	0,997	0,992	0,976	0,997	0,987	0,958	0,996	0,974	0,926	0,991

(b) Intraclass Correlation for intra- and inter-observer agreement of calculated SL and CL angles

Experiment	Angle	Intra-observer 1	95% Confidence Interval		Intra-observer 2	95% Confidence Interval		Inter-observer 1	95% Confidence Interval		Inter-observer 2	95% Confidence Interval	
		ICC	Lower bound	Upper bound	ICC	Lower bound	Upper bound	ICC	Lower bound	Upper bound	ICC	lower bound	Upper bound
No movement, low dosage	SL	0,885	0,600	0,970	0,807	0,412	0,948	0,909	0,625	0,978	0,955	0,989	0,989
	CL	0,988	0,953	0,997	0,968	0,886	0,992	0,988	0,938	0,997	0,983	0,997	0,997
No movement, high dosage	SL	0,835	0,429	0,957	**0,600**	0,049	0,880	**0,729**	0,015	0,931	0,835	0,958	0,958
	CL	0,993	0,933	0,998	0,979	0,923	0,995	0,985	0,778	0,997	0,984	0,997	0,997
FE, low speed	SL	0,942	0,874	0,974	0,943	0,874	0,974	0,950	0,887	0,978	0,962	0,983	0,983
	CL	0,989	0,975	0,995	0,982	0,959	0,992	0,993	0,985	0,997	0,992	0,997	0,997
RUD, low speed	SL	0,980	0,957	0,991	0,941	0,874	0,973	0,976	0,885	0,992	0,972	0,992	0,992
	CL	0,997	0,994	0,999	0,982	0,961	0,992	0,991	0,979	0,996	0,992	0,997	0,997
FE, high speed	SL	0,912	0,733	0,973	0,959	0,865	0,988	0,962	0,860	0,984	0,932	0,674	0,982
	CL	0,990	0,971	0,996	0,978	0,928	0,993	0,981	0,889	0,997	0,955	0,785	0,988
RUD, high speed	SL	0,934	0,818	0,977	0,896	0,734	0,962	0,955	0,870	0,989	0,965	0,819	0,990
	CL	0,986	0,951	0,996	0,986	0,960	0,995	0,990	0,964	0,995	0,983	0,901	0,995

SL, Scapholunate; CL, Capitolunate; ICC, Intraclass correlation. Values below 0.75 are in bold. 95% CI values are boldened if they go below 0. Intra-observer 1 and 2 show the intra-observer agreement of rater 1 and 2 respectively. Inter-observer 1 and 2 show the agreement between rater 1 and 2 for the first and second measurements respectively.

Table 4.3: Intraclass correlation for intra- and interobserver agreement of select scaphoid measurements including the third observer

Experiment	Bone measured	Intra-observer 3	95% CI		Inter-observer 1	95% CI		Inter-observer 2	95% CI	
		ICC	Lower bound	Upper bound	ICC	Lower bound	Upper bound	ICC	Lower bound	Upper bound
No movement, low dosage	Scaphoid	**0,588**	**-0,009**	0,878	**0,505**	**-0,496**	0,868	0,783	0,373	0,941
No movement, high dosage	Scaphoid	0,865	0,540	0,965	0,933	0,788	0,982	0,926	0,732	0,981
RUD, low speed	Scaphoid	0,925	0,842	0,966	0,893	0,763	0,952	0,907	0,782	0,959
RUD, high speed	Scaphoid	**0,490**	0,049	0,781	**0,749**	0,361	0,908	0,889	0,721	0,959

ICC, Intraclass correlation. Values below 0.75 are in bold. 95% CI values are boldened if they go below 0. Intraobserver 3 shows the intra-observer agreement of rater 3. Inter-observer 1 and 2 show the agreement between rater 1, 2 and 3 for the first and second measurements respectively.

5 Discussion

Decisions were made in the design of the motion device, as well as in the process leading up to the experiments and data analysis. These have produced results which will be discussed in this chapter. Furthermore, there are opportunities to bring the design and its use to a higher level. In this chapter, an analysis of the results from chapter 4 will follow. After this, some limitations of this study will be discussed. Finally, recommendations for future research will be provided.

5.1. Analysis

5.1.1. Design optimalizations

Based on the literature, this is the first time that the design process of a motion guidance device for the wrist is reported at this level of detail. This makes it difficult to compare the design process and in some ways the results with the current scientific sources. Next to the main goal, which was the standardization of movement, the design goals have all been met. During the experiments, the motors proved powerful enough and both FE and RUD could be performed at different speeds. No artefacts due to non-radiolucent materials were present on the images, and arms of different sizes fitted and could be moved. Furthermore, during the design process, the modular nature of the device proved invaluable in rapid prototyping, having the ability to swap out parts easily and quickly. It also allowed for easy transport, storage, and cleaning.

Despite reaching its goals, there are several things that were noted during and after the experiments which ask for further investigation and improvement of the device. First, the lack of stiffness of the PMMA parts. This was also noticed before the start of the experiment with cadaveric samples and a set of new parts were designed and laser cut to counteract this phenomenon. These parts did however not arrive in time to be installed before the experiments. This set of parts is shown in fig. 5.1, and should improve the stiffness of the device greatly, counteracting this effect. The nylon bolts that were used as axes also did not prove stiff enough, especially the longer ones (60mm). When put under load these axes would bend. By using axes made of a stiffer material, for example carbon, this can be negated.

Second, a better way has to be found to attach the hands to the bar. During the experiments, the friction and weight of the hands were deemed enough to be able to produce movement. However, there were still some motion artefacts present, even in the slower-moving images, which could be explained by the slipping of the hand on the bar. In live subjects, this does not offer as much of a problem, as they can hold the bar themselves. However, in the case of cadaveric experiments, it would be wise to think of a way to attach the hands to the bar more sturdily.

Third, the RUD movement should be optimized. Better gearing should be introduced instead of the 3D-printed double gear. The twisted timing belt should not have as much of a curve towards the middle and move in a more direct line towards the gear on top. Finally, the RUD movement should be able to be locked. This can be done in the software by locking or counter-rotating the RUD motor, or mechanically, for example with a pin which locks the sideways rotation of the hand carriage when desired.

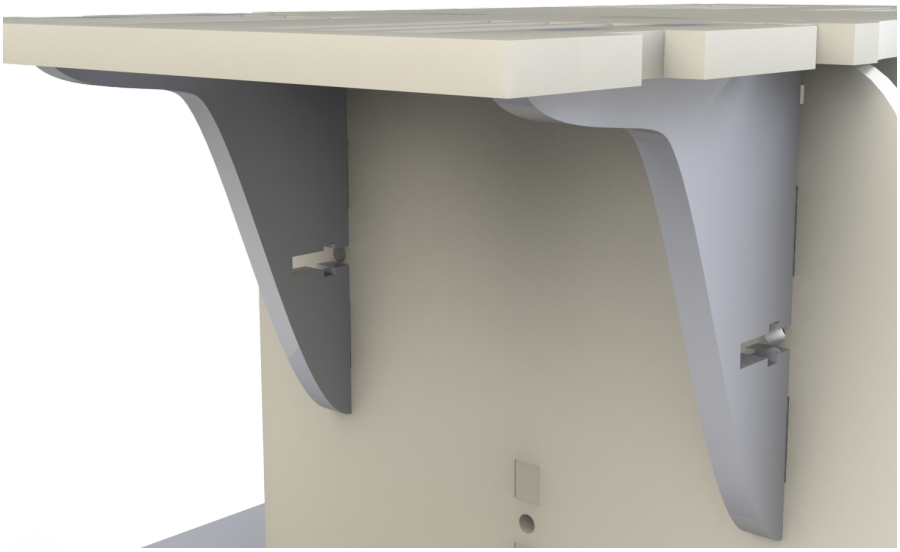

Figure 5.1: Lasercut supporting parts to counter flexing of PMMA due to weight of a specimen (grey). Frontal view with several parts hidden for clarity.

While these improvements might not have an immediate visible effect on the reliability of the produced images, they will have a large impact on the robustness and use of the device. Especially the improved stiffness of the device should ensure a more efficient and smooth transfer of motion from the motors to the wrist, resulting in smoother movement and less unpredictable motion artefacts.

5.1.2. Experiments and effects of scan parameters

As pointed out in chapter 4.2, three samples were used but only two were included in the data. The third sample showed significant damage to the carpal bones with visible open scars and very porous bones. Furthermore, the specimen was extremely stiff, only moving a few degrees with each movement. Because of the lack of movement, this specimen was not used in data analysis since they were essentially static images. This did however reduce the number of cadaveric samples to two, which is statistically less desirable.

The scan parameters that were varied were radiation dosage and motion speed. The varied variables were taken from similar literature to come up with a scan protocol. For standardization, it is important to use common values and to report the findings of these varied variables, as this might lead to insight into an optimal way to measure wrist kinematics. While the overall reported ICCs were good to excellent, it should be noted that in particular, the ICC for the scaphoid with low radiation dosage was significantly lower than the rest. While it is important to keep the exposure to radiation under certain limits, there should not be a significant reduction in image quality. However, in using a (higher) tube current of 80 mA, the effective dosage still only reaches 0.08 mSv with the current scan protocol. This is far below the yearly limit of 1.0 mSv, and thus should be no problem.

Motion speed showed a less visible effect on the reliability of images. It was assumed that with higher speed and more motion artefacts, reliability would drop. This is somewhat visible in the ICCs, with a few lower bounds dropping under 0.75, however, did not have as big as an influence as expected. A possible explanation is that images with lower quality, such as high-speed movements, are more difficult to measure. This might mean that the observers 'tried harder' with these images to do it right, as it was not a matter of quickly drawing a clear line.

5.1.3. Post-processing and ICCs

Based on the results reported in chapter 4 in table 4.2, the motion device helped in getting reliable measurements of the angles of the carpal bones. Comparing the ICC values with those found in literature is not easy. First, there are not many papers reporting the ICCs for the angle of interest. Secondly, when finding papers which do report the ICC of these angles, often the ICC is reported poorly. ICC type,

as well as lower and upper limits of the 95% confidence interval, are frequently lacking. This makes it difficult to compare the found ICC values in this thesis.

Perhaps the most comparable is the work of Tan et al. [37], who measured SL, CL, radiolunate, and radioscaphoid angles on MRI, radiographs and CT scans, although they do measure angles slightly differently. The ICC was used to measure both inter- and intraobserver reliability, however, no ICC type was mentioned. Lunate intra-observer agreement was reported with an ICC of 0.96 (0.91-0.99), and interobserver agreement 0.92 (0.81 - 0.97). These values are quite high, and similar to the values found in this thesis, where lunate ICC values are also very high across all scans. Scaphoid intra-observer agreement was reported with an ICC of 0.89 (0.73-0.96) and an inter-observer agreement of 0.88 (0.71 - 0.95), again comparable with most of the values found in this thesis, except for the scan with no movement and low dosage. SL angle ICCs (Intra-observer 0.88 (0.71 - 0.95) and inter-observer 0.84 (0.61 - 0.94)) and CL angle ICCs (Intra-observer 0.66 (0.18 – 0.86) and inter-observer 0.85 (0.63 – 0.94) were both found to be similar if not lower than the values reported in table 4.2b.

Other studies reported similar or lower ICCs. Arab et al. reported an ICC of 0.85 (0,82 - 0,87) for measured SL dissociation, which effectively is the distance between the scaphoid and lunate, during RUD [38]. Suzuki et al. reported the ICC for measured SL distance, with an interrater ICC of 0,730 and an intrarater ICC of 0,832 [39]. Park et al. reported the ICC of the intrascaphoid angle (ISA), SLA and scaphohamate angle (SHA) pre- and postoperatively [40]. The reliability for ISA angles measured pre- and postoperatively are low, 0,509 (0,247 - 0,691) and 0,292 (-0,87 - 0,554) respectively. SLA and SHA reliability is higher though, with an ICC averaging above 0,9. None of these papers reported ICC type.

When comparing the values mentioned above with those found in this study, a few things stand out.

First of all, The ICC values of this study almost all are similar if not higher when compared to values reported in the literature, and are almost all good to excellent following Koo et al. [34]. Especially the values for scans of moving wrists are high. A possible explanation for this result is the fact that the combination of the motion device and 4D CT scanning delivers as reliable if not more reliable images than X-ray scanning, which is the most used imaging method to measure SL and CL angles.

Secondly, intra- and inter-observer agreement in the same measurement is similar in almost all cases. Because of the fact that the measurement rules were very clear, and lower intra-observer agreement was often paired with the lower inter-observer agreement, this supports the assumption that the effects seen in the ICCs are due to the image quality, and not any other factors such as the medical experience of the raters, the fact that raters could have 'learned' to do measurements as they were going, and other possible effects.

Thirdly, all ICC values lower than 0.75, and thus having worse reliability than "good", are from measurements of the scaphoid. This is the case for both intra- and inter-observer agreement. Especially in the static scan with a low dosage and during RUD movements, the ICC was low for this carpal bone. Although this might seem strange at first, since static images should logically provide the highest agreement, there are several factors that can explain this deviation. The rules on how to measure the bones were communicated clearly to each observer. However, the scaphoid presents a complex anatomy, especially when the bone is quite porous, and the borders between bones get less visible. This is often the case in cadaveric specimens. This could explain the lower agreement.

The lower scaphoid reliability is also visible in the calculated SL angles from table 4.2b. CL angles all provide excellent reliability, while multiple SL ICCs are significantly lower. This is also in contrast with the values found in the literature mentioned above. When looking at the case of wrist instability, this finding might have a significant impact. A large part of the diagnosis of dynamic wrist instabilities is based on SL angle measurements. If the intra- and inter-observer agreement for scaphoid angle are low, then the SL angle might be an unreliable metric for this diagnosis. Further research should be conducted on why the scaphoid measurements were more unreliable than the other bones.

Finally, when looking at the ICC values of the third observer in table 4.3, a few things should be discussed. First, the scaphoid value for no movement and low dosage is very low, comparable with the values of the first and second raters. This shows that this issue is not coming from the raters, but could be coming from image quality or difficulties due to the scaphoid anatomy. Second, the intra-observer agreement for high-speed RUD is significantly lower than with the first two observers. Lastly, the inter-observer agreement for the second measurement is higher for most of the measurements than the agreement for the first measurement. An explanation for this could be that the raters slowly 'got better' at measuring. However this effect is not as visible with the first two raters, and the third rater was an

orthopaedic surgeon who has done this kind of measurement thousands of times. The only thing which differed from the first two observers was the fact that the third observer had to rate fewer images than the first and second raters. It would therefore be advisable to repeat these measurements with the full set of images for the third observer.

5.2. Limitations

Naturally, there are some limitations to this thesis which could influence the results. A point could be made that not the performance of the device is measured, but the measurement skills of the raters. However, as touched on before, since the rules of measurement were very clear, and since both intra- and inter-observer agreement was measured and was found to be very similar in the same measurements, it is assumed that the effects visible in the ICC are mainly caused by the images and their quality, and not by the (lack of) experience and skill of the raters.

Secondly, only two cadaveric specimens were included in the analysis. This makes the statistical value less than it would have been with three or more samples. However, since the variable of interest is not the actual angle measurement between specimens or in a population, but the agreement between measures, this is not as big a problem. It is unlikely that specimens themselves could have a large impact on the measurement agreement. The uncertainty and difference in stiffness sadly is however the reality of cadaveric experiments.

Thirdly, it can be said that the focus lies too much on the dynamic instability as a case, and too little on the more generic use of the device. Although a valid point of critique, it was thought that if the device can produce reliable images for this pathology, this result should be able to be extrapolated to other pathologies and use cases in the wrist.

Lastly, in isolating the radiation dosage variable, the choice was made to not move the wrist while doing so, similar to an experiment carried out by Dobbe et al. [12]. It would however be insightful to also see what kind of effect the radiation dosage has on image quality if the sample is moving.

5.3. Recommendations

Following the limitations in the previous section, firstly it is naturally advised to implement the design improvements discussed in section 5.1.1. Also, for the purpose of prototyping, it is fine to laser-cut parts. However, when used more frequently or in clinical settings, it is advised to use injection moulded parts. This reduces sharp edges and corners and enables more easy cleaning with smoother surfaces and less bolted connections.

For further research using this kind of device with 4D scanning of the wrist, it is highly encouraged to experiment with different cases and carpal bones to identify the best use cases for this kind of device. It is advised to especially explore the visibility and measurement protocols for the scaphoid bone since some of the ICC values were particularly low.

Future research is also recommended to use a segmentation and registration algorithm to (semi) automatically analyze the kinematics of the wrist. Such an algorithm could greatly decrease the amount of work needed to analyze the data, as well as provide a lot more data automatically such as all carpal bone angles during all frames, their surface contacts, and many more.

Furthermore, it would be interesting to experiment with what effects different pathologies have on the kinematics of the wrist and include specimens or patients with these pathologies. It would also be beneficial to increase the sample size of specimens to more than two. Increasing the number of raters measuring the images will give more data points to better evaluate the usability of the images. As for the standardization of the movements and scans, there is much to be gained here. While this device provides some kind of standardization in its placement and movement, it has become clear that standardization is much more than that. It is imperative that clear and standardized scanning protocols should be devised. Although hospitals will have their own protocols, no 'golden standard' exists for 4D CT scanning with a set motion speed, radiation dosage, movements of interest, and more. The effect of these factors was lightly touched upon in this work, but should definitely be explored further. Also, the different movements, placement of the hand, and other factors should be specified further to truly standardize these movements.

6

Conclusion

This thesis produced a usable motion guidance device for the wrist which has the potential to be used in a 4D CT scanning environment. The designed motion guidance device was successful in performing FE and RUD during 4D CT scans, which was an important goal. Furthermore, steps have been taken towards the standardization of movement, however, there is still much to be gained in the standardization of movement. The device, in combination with a CT scanner, produced usable 4D CT images which are interpretable and can be used to measure and analyze carpal angles and kinematics. These kinds of devices provide a new and exciting platform in the world of dynamic scanning. The value of standardization in this process can not be understated, providing a basis for future experiments and possibly diagnostic protocols.

The main goal of this thesis as described in section 2.3 was to design a motorized motion guidance device for the wrist which can be used in a 4D CT scanner environment. The main research question was aimed at finding out if this designed device can yield reliable 4D CT images which can be used in various analyses of the wrist. Three subquestions which arose from this question were as follows:

1. How should a motion guidance device with the goal of yielding reliable 4D CT images be designed?
2. How can the 4D CT scans made in combination with this device best be performed?
3. How can the reliability of the retrieved 4D CT images of a wrist in motion be tested?

The main goal of this thesis was achieved. A motorized motion guidance device for the wrist, which can be used in conjunction with a 4D CT scanner was designed. To answer the main question: Yes, a motion guidance device can yield reliable images to be used in the kinematic analysis of the wrist. ICC values for measured and calculated angles were mostly good to excellent.

To answer the first subquestion, a motorized motion guidance device for the wrist was designed which performs FE and URD of the wrist with different speeds. It is fully modular and can be disassembled and repaired very easily. Driven by two stepper motors and a microcontroller, it standardizes the placement and motion of the wrist inside a 4D CT scanning environment. Second, to validate the reliability of images produced by the device in combination with a 4D CT scanner and to optimize its use, an experiment consisting of several different scans was performed. Three cadaveric samples were scanned during different movements and radiation dosages to find their effect on image reliability. Two of these samples moved expected amounts, while the third was too stiff to show more movement than a few degrees. During the experiments, it became apparent that some weaknesses in the design were present, among which the stiffness of the PMMA parts and several issues in the RUD movement. Thirdly, to test the reliability of the retrieved 4D CT images, scaphoid, lunate and capitate angles were measured twice by two raters. From these angles, SLA and CLA were calculated. ICCs of all of these angles were calculated. Overall, ICC for SLA and CLA is good to excellent, especially in FE measurements. The scaphoid angle was deemed the most troublesome, resulting in the lowest ICCs, particularly in scans with no movement and low radiation dosage. For verification, a third rater measured the scans with the lowest ICCs twice too, resulting in more or less the same results with especially low ICC values for static, low-dosage scans.

This thesis study aimed to design a motorized motion guidance device for the wrist, which can be used with 4D CT scans. These scans can then be used for various wrist-related analyses in research or in the future even in clinical applications. This kind of device is needed because there is a lack of standardization in the use of 4D CT for the wrist. This thesis takes the first steps towards standardizing these experiments and measurements for the wrist, showing that reliable images can indeed be acquired from a 4D CT scanner in combination with this device. It presents a motion guidance device which performs motorized FE and RUD and is fully modular to be improved in the future. This kind of device can bring huge benefits, giving insights into the largely unknown carpal kinematics. In the future, such devices might even be used in clinical settings, providing images which can be used in the diagnosis of dynamic carpal instabilities, or analysing the kinematics of a freshly placed lunate implant.

References

[1] M. J. Rainbow, A. L. Wolff, J. J. Crisco, and S. W. Wolfe, "Functional kinematics of the wrist," *J Hand Surg Eur Vol*, vol. 41, no. 1, pp. 7–21, 2016, ISSN: 0266-7681. DOI: 10.1177/1753193415616939.

[2] H. Stoesser, C. E. Padmore, M. Nishiwaki, B. Gammon, G. D. G. Langohr, and J. A. Johnson, "Biomechanical evaluation of carpal kinematics during simulated wrist motion," *J Wrist Surg*, vol. 6, no. 2, pp. 113–119, 2017, ISSN: 2163-3916 (Print) 2163-3916. DOI: 10.1055/s-0036-1588025.

[3] M. Brinkhorst *et al.*, "Four-dimensional ct analysis of carpal kinematics: An explorative study on the effect of sex and hand-dominance," *J Biomech*, p. 110 870, 2021, ISSN: 0021-9290. DOI: 10.1016/j.jbiomech.2021.110870.

[4] T. M. Moojen, J. G. Snel, M. J. Ritt, H. W. Venema, J. M. Kauer, and K. E. Bos, "In vivo analysis of carpal kinematics and comparative review of the literature," *J Hand Surg Am*, vol. 28, no. 1, pp. 81–7, 2003, ISSN: 0363-5023 (Print) 0363-5023. DOI: 10.1053/jhsu.2003.50009.

[5] M. Brinkhorst *et al.*, "Quantifying in vivo scaphoid, lunate, and capitate kinematics using four-dimensional computed tomography," *Skeletal Radiol*, vol. 50, no. 2, pp. 351–359, 2021, ISSN: 0364-2348 (Print) 0364-2348. DOI: 10.1007/s00256-020-03543-4.

[6] B. Akhbari, A. M. Morton, D. C. Moore, A. C. Weiss, S. W. Wolfe, and J. J. Crisco, "Accuracy of biplane videoradiography for quantifying dynamic wrist kinematics," *J Biomech*, vol. 92, pp. 120–125, 2019, ISSN: 0021-9290 (Print) 0021-9290. DOI: 10.1016/j.jbiomech.2019.05.040.

[7] F. D. Kerkhof *et al.*, "Quantifying thumb opposition kinematics using dynamic computed tomography," *J Biomech*, vol. 49, no. 9, pp. 1994–1999, 2016, ISSN: 0021-9290. DOI: 10.1016/j.jbiomech.2016.05.008.

[8] G. I. Bain *et al.*, "The effect of lunate morphology on the 3-dimensional kinematics of the carpus," *J Hand Surg Am*, vol. 40, no. 1, 81–9.e1, 2015, ISSN: 0363-5023. DOI: 10.1016/j.jhsa.2014.09.019.

[9] S. B. M. MacLean and G. I. Bain, "Kinematics of the wrist in kienböck's disease: A four-dimensional computed tomography study," *J Hand Surg Eur Vol*, vol. 46, no. 5, pp. 504–509, 2021, ISSN: 0266-7681. DOI: 10.1177/1753193420987790.

[10] M. G. A. de Roo, J. G. G. Dobbe, C. van der Horst, G. J. Streekstra, and S. D. Strackee, "Carpal kinematic changes after scaphoid nonunion: An in vivo study with four-dimensional ct imaging," *J Hand Surg Eur Vol*, vol. 44, no. 10, pp. 1056–1064, 2019, ISSN: 1753-1934 (Print) 0266-7681. DOI: 10.1177/1753193419866598.

[11] S. Kakar *et al.*, "The role of dynamic (4d) ct in the detection of scapholunate ligament injury," *J Wrist Surg*, vol. 5, no. 4, pp. 306–310, 2016, ISSN: 2163-3916 (Print) 2163-3916. DOI: 10.1055/s-0035-1570463.

[12] J. G. G. Dobbe, M. G. A. de Roo, J. C. Visschers, S. D. Strackee, and G. J. Streekstra, "Evaluation of a quantitative method for carpal motion analysis using clinical 3-d and 4-d ct protocols," *IEEE Trans Med Imaging*, vol. 38, no. 4, pp. 1048–1057, 2019, ISSN: 1558-254X (Electronic) 0278-0062 (Linking). DOI: 10.1109/TMI.2018.2877503.

[13] M. Garcia-Elias, X. Alomar Serrallach, and J. Monill Serra, "Dart-throwing motion in patients with scapholunate instability: A dynamic four-dimensional computed tomography study," *J Hand Surg Eur Vol*, vol. 39, no. 4, pp. 346–52, 2014, ISSN: 0266-7681. DOI: 10.1177/1753193413484630.

[14] K. K. Wang, X. Zhang, D. McCombe, D. C. Ackland, E. T. Ek, and S. K. Tham, "Quantitative analysis of in-vivo thumb carpometacarpal joint kinematics using four-dimensional computed tomography," *J Hand Surg Eur Vol*, vol. 43, no. 10, pp. 1088–1097, 2018, ISSN: 0266-7681. DOI: 10.1177/1753193418789828.

[15] M. Brinkhorst, G. Streekstra, J. van Rosmalen, S. Strackee, and S. Hovius, “Effects of axial load on in vivo scaphoid and lunate kinematics using four-dimensional computed tomography,” *J Hand Surg Eur Vol*, vol. 45, no. 9, pp. 974–980, 2020, ISSN: 1753-1934 (Print) 0266-7681. DOI: 10.1177/1753193420943400.

[16] I. S. Mat Jais and S. C. Tay, “Kinematic analysis of the scaphoid using gated four-dimensional ct,” *Clin Radiol*, vol. 72, no. 9, 794.e1–794.e9, 2017, ISSN: 0009-9260. DOI: 10.1016/j.crad.2017.04.005.

[17] D. Bakker *et al.*, “Is midcarpal arthroscopy for suspected scapholunate pathology associated with greater interobserver agreement and more frequent offer of surgery?” *J Hand Surg Am*, 2022, ISSN: 1531-6564 (Electronic) 0363-5023 (Linking). DOI: 10.1016/j.jhsa.2022.07.001. [Online]. Available: https://www.ncbi.nlm.nih.gov/pubmed/36031464.

[18] J. White, G. Couzens, and C. Jeffery, “The use of 4d-ct in assessing wrist kinematics and pathology: A narrative view,” *Bone Joint J*, vol. 101-b, no. 11, pp. 1325–1330, 2019, ISSN: 2049-4394. DOI: 10.1302/0301-620x.101b11.Bjj-2019-0361.R1.

[19] S. K. Lee, H. Desai, B. Silver, G. Dhaliwal, and N. Paksima, “Comparison of radiographic stress views for scapholunate dynamic instability in a cadaver model,” *J Hand Surg Am*, vol. 36, no. 7, pp. 1149–57, 2011, ISSN: 1531-6564 (Electronic) 0363-5023 (Linking). DOI: 10.1016/j.jhsa.2011.05.009.

[20] P. N. D’Ailly, N. W. Schep, and J. Coert, “Artroscopie van de pols,” *Ned Tijdschr Geneeskd.*, vol. 166, no. D6312, 2022.

[21] J. K. Andersson, “Treatment of scapholunate ligament injury: Current concepts,” *EFORT Open Rev*, vol. 2, no. 9, pp. 382–393, 2017, ISSN: 2058-5241 (Print) 2058-5241. DOI: 10.1302/2058-5241.2.170016.

[22] A. Kitay and S. W. Wolfe, “Scapholunate instability: Current concepts in diagnosis and management,” *J Hand Surg Am*, vol. 37, no. 10, pp. 2175–96, 2012, ISSN: 0363-5023. DOI: 10.1016/j.jhsa.2012.07.035.

[23] W. Geissler, “Wrist arthroscopy,” in 2015. DOI: 10.1016/B978-1-4557-7427-2.00017-4.

[24] A. K. Chong, J. X. Lim, and D. M. Tan, “Diagnostic imaging of the hand and wrist,” in ch. 3. DOI: 10.1016/B978-0-323-35712-8.00003-5.

[25] R. Carr, S. MacLean, J. Slavotinek, and G. I. Bain, “Four-dimensional computed tomography scanning for dynamic wrist disorders: Prospective analysis and recommendations for clinical utility,” *J Wrist Surg*, vol. 8, no. 2, pp. 161–167, 2019, ISSN: 2163-3916 (Print) 2163-3916 (Linking). DOI: 10.1055/s-0038-1675564.

[26] Y. S. Choi, Y. H. Lee, S. Kim, H. W. Cho, H. T. Song, and J. S. Suh, “Four-dimensional real-time cine images of wrist joint kinematics using dual source ct with minimal time increment scanning,” *Yonsei Med J*, vol. 54, no. 4, pp. 1026–32, 2013, ISSN: 0513-5796 (Print) 0513-5796. DOI: 10.3349/ymj.2013.54.4.1026.

[27] S. Leng, K. Zhao, M. Qu, K. N. An, R. Berger, and C. H. McCollough, “Dynamic ct technique for assessment of wrist joint instabilities,” *Med Phys*, vol. 38 Suppl 1, S50, 2011, ISSN: 2473-4209 (Electronic) 0094-2405 (Linking). DOI: 10.1118/1.3577759. [Online]. Available: https://www.ncbi.nlm.nih.gov/pubmed/21978117.

[28] I. S. Mat Jais, X. Liu, K. N. An, and S. C. Tay, “A method for carpal motion hysteresis quantification in 4-dimensional imaging of the wrist,” *Med Eng Phys*, vol. 36, no. 12, pp. 1699–703, 2014, ISSN: 1350-4533. DOI: 10.1016/j.medengphy.2014.08.011.

[29] J. R. Schiller, J. J. Brooks, P. K. Mansuripur, J. A. Gil, and E. Akelman, “Three-dimensional carpal kinematics after carpal tunnel release,” *J Wrist Surg*, vol. 5, no. 3, pp. 222–6, 2016, ISSN: 2163-3916 (Print) 2163-3916. DOI: 10.1055/s-0036-1578812.

[30] A. de Lange, J. M. Kauer, and R. Huiskes, “Kinematic behavior of the human wrist joint: A roentgen-stereophotogrammetric analysis,” *J Orthop Res*, vol. 3, no. 1, pp. 56–64, 1985, ISSN: 0736-0266 (Print) 0736-0266 (Linking). DOI: 10.1002/jor.1100030107.

[31] C. P. Neu, J. J. Crisco, and S. W. Wolfe, “In vivo kinematic behavior of the radio-capitate joint during wrist flexion-extension and radio-ulnar deviation,” *J Biomech*, vol. 34, no. 11, pp. 1429–38, 2001, ISSN: 0021-9290 (Print) 0021-9290. DOI: 10.1016/s0021-9290(01)00117-8.

[32] *3D Slicer image computing platform*. [Online]. Available: https://www.slicer.org/.

[33] A. Fedorov *et al.*, “3d slicer as an image computing platform for the quantitative imaging network,” *Magn Reson Imaging*, vol. 30, no. 9, pp. 1323–41, 2012, ISSN: 1873-5894 (Electronic) 0730-725X (Linking). DOI: 10.1016/j.mri.2012.05.001. [Online]. Available: https://www.ncbi.nlm.nih.gov/pubmed/22770690.

[34] T. K. Koo and M. Y. Li, “A guideline of selecting and reporting intraclass correlation coefficients for reliability research,” *J Chiropr Med*, vol. 15, no. 2, pp. 155–63, 2016, ISSN: 1556-3707 (Print) 1556-3715 (Electronic) 1556-3707 (Linking). DOI: 10.1016/j.jcm.2016.02.012.

[35] R. Perneder and I. Osborne, *Handbook Timing Belts: principles, calculations, applications*. Springer Science & Business Media, 2012, ISBN: 978-3-642-17754-5. DOI: 10.1007/978-3-642-17755-2.

[36] *Pololu - DRV8825 Stepper Motor Driver Carrier, High Current*. [Online]. Available: https://www.pololu.com/product/2133.

[37] S. Tan, S. S. Ghumman, M. Ladouceur, and T. P. Moser, “Carpal angles as measured on ct and mri: Can we simply translate radiographic measurements?” *Skeletal Radiol*, vol. 43, no. 12, pp. 1721–8, 2014, ISSN: 1432-2161 (Electronic) 0364-2348 (Linking). DOI: 10.1007/s00256-014-1994-3. [Online]. Available: https://www.ncbi.nlm.nih.gov/pubmed/25194938.

[38] W. Abou Arab *et al.*, “Scapholunate instability: Improved detection with semi-automated kinematic ct analysis during stress maneuvers,” *Eur Radiol*, vol. 28, no. 10, pp. 4397–4406, 2018, ISSN: 1432-1084 (Electronic) 0938-7994 (Linking). DOI: 10.1007/s00330-018-5430-2. [Online]. Available: https://www.ncbi.nlm.nih.gov/pubmed/29713765.

[39] D. Suzuki *et al.*, “Comparison of scapholunate distance measurements on plain radiography and computed tomography for the diagnosis of scapholunate instability associated with distal radius fracture,” *Journal of Orthopaedic Science*, vol. 19, no. 3, pp. 465–470, 2014, ISSN: 0949-2658. DOI: https://doi.org/10.1007/s00776-014-0533-3. [Online]. Available: https://www.sciencedirect.com/science/article/pii/S0949265815302736.

[40] H. Y. Park, J. O. Yoon, K. Kim, K. Bae, D. W. Sohn, and J. S. Kim, “Reliability of semi-pronated ulnar deviation pa view (billiard view) of the wrist in evaluating the scaphoid,” *J Plast Reconstr Aesthet Surg*, vol. 69, no. 7, pp. 977–82, 2016, ISSN: 1878-0539 (Electronic) 1748-6815 (Linking). DOI: 10.1016/j.bjps.2016.02.013. [Online]. Available: https://www.ncbi.nlm.nih.gov/pubmed/27053512.

A

Experimental Protocol

Cadaver Study Protocol Evaluation 4D CT scan device

Protocol Version	1.0
Study date	26/07/2022
Study Location	Reinier de Graaf Gasthuis
Goals of the study	To validate a 4D CT scanning device for the wrist.
Participants	

General Timeline

Time	**Task**	**Participants**
17:00	Get specimens from Erasmus	
17:30	Gathering at RDGG (with specimens)	
17:45	Setup Device, CT scanner and specimens	
18:15	Perform measurements and 4D CT scans on Specimen 1	
19:00	Perform measurements and 4D CT scans on Specimen 2	
19:45	Perform measurements and 4D CT scans on Specimen 3	
-	Time in case something goes wrong	
20:45	Breakdown and cleanup	
21:00	Return specimens to Erasmus	

Supplies

Wetlab EMC			
Check	**Materials**	**Location**	**Responsible**
☐	3 cadaveric specimens of the wrist	Wetlab EMC	
☐	Covering material	Wetlab EMC	
RDGG CT Room			
Check	**Materials**	**Location**	**Responsible**
☐	CT Scanner	RDGG	
☐	External Hard Drive	TU	
☐	Movement guidance Device		
☐	Tools to place specimen in device and attach (Velcro straps + Chinese fingers)		
☐	Power Extension cord		
☐	Screwdriver and replacement parts for device + extra wires		
☐	1x Board to place device on		
☐	Tie wraps		
☐	Duct-tape		
☐	Laptop and charger		
☐	USB-B to USB-A cable		
☐	Photo-camera		
☐	Notebook		
☐	Gloves	RDGG	
☐	Instant glue		
☐	Plastic bags (for storage of anything)		
☐	Permanent marker		
☐	Table/trolley (for temporary storage of specimens)	RDGG	
☐	Scissors		
☐	Prints of this protocol		
☐	Tools for cleaning	RDGG	
☐			
☐			

Appendix A: Experiment protocols

Room: CT room at the RDGG

Participants:

1. Setup:

1. Cover the CT table
2. Place Board
3. Make sure all wires of the device are attached correctly[WC1] (Appendix D)
4. Place Device on board and attach with tie wraps in the holes drilled in the board and at the bottom of the feet of the device. (Appendix E)
5. Mark the specimens (1,2,3) and make a photo in dorsal view of all three.

2. Place Specimen

1. Wear gloves
2. Place specimen 1 in the device with the hand palm surrounding the white bar
3. Attach specimen to device with Velcro straps and Chinese fingers

3. Positional accuracy measurements

1. Attach power to the device (by plugging it into the extension cord)
2. Move device to location 1 (see table I) by pressing button 1
3. Measure the location reached with a goniometer and note in table I
4. Reset location and repeat measurement twice
5. Repeat step 3.2-3.4 for all 4 locations

4. 4D CT scans

1. Place device with specimen on the board in the CT scanner
2. Make a 4D CT scan of non-moving wrist with low radiation dosage
   (See appendix C.1 for scan protocol)
3. Check table II
4. Make a 4D CT scan of non-moving wrist with default radiation dosage
   (See appendix C.2 for scan protocol)
5. Check table II
6. Let the device perform Flexion/Extension (FE) with low speed (27° per second)
7. Make 4D CT scan of moving wrist with low speed
   (See appendix C.2 for scan protocol)
8. Check table II
9. Let the device perform Ulnar/Radial Deviation (URD) with low speed (27° per second)
10. Make 4D CT scan of moving wrist with low speed
    (See appendix C.2 for scan protocol)
11. Check table II
12. Let the device perform Flexion/Extension (FE) with high speed (90° per second)
13. Make 4D CT scan of moving wrist (FE) with high speed
    (See appendix C.2 for scan protocol)
14. Check table II
15. Let the device perform Ulnar/Radial Deviation (URD) with high speed (90° per second)
16. Make 4D CT scan of moving wrist (URD) with high speed
    (See appendix C.2 for scan protocol)
17. Check table II

5. Replace specimen:
    1. Remove power
    2. Detach specimen 1 from device
    3. Place specimen 2 in device as described in step 2. (Place Specimen)
    4. Repeat step 3. (Positional accuracy measurements) for and step 4 (4D CT scans) for specimen 2
    5. Repeat step 5.1-5.4 for specimen 3
6. End of experiment
    1. Remove power
    2. Detach last specimen
    3. Clean up device, CT table and CT room
    4. Copy CT files to external hard drive
    5. Cover and store specimens

TABLE II

Ct Scan	Done?	Notes
Specimen 1 low dosage	☐	
Specimen 1 high dosage	☐	
Specimen 1 low speed FE	☐	
Specimen 1 low speed URD	☐	
Specimen 1 high speed FE	☐	
Specimen 1 high speed URD	☐	
Specimen 2 low dosage	☐	
Specimen 2 high dosage	☐	
Specimen 2 low speed FE	☐	
Specimen 2 low speed URD	☐	
Specimen 2 high speed FE	☐	
Specimen 2 high speed URD	☐	
Specimen 3 low dosage	☐	
Specimen 3 high dosage	☐	
Specimen 3 low speed FE	☐	
Specimen 3 low speed URD	☐	
Specimen 3 high speed FE	☐	
Specimen 3 high speed URD	☐	

Appendix C: CT Protocols low and default dosage

C.1 Low radiation dosage

Variable	**Value**
Tube Current	15 mA
Tube Potential	80 kV
Total ScanTime	12.6 s
Range	140.0 mm
DFoV	120.0 mm

C.2 Default radiation dosage

Variable	**Value**
Tube Current	80 mA
Tube Potential	80 kV
Total ScanTime	12.6 s
Range	140.0 mm
DFoV	120.0 mm

Appendix D: Arduino Wiring

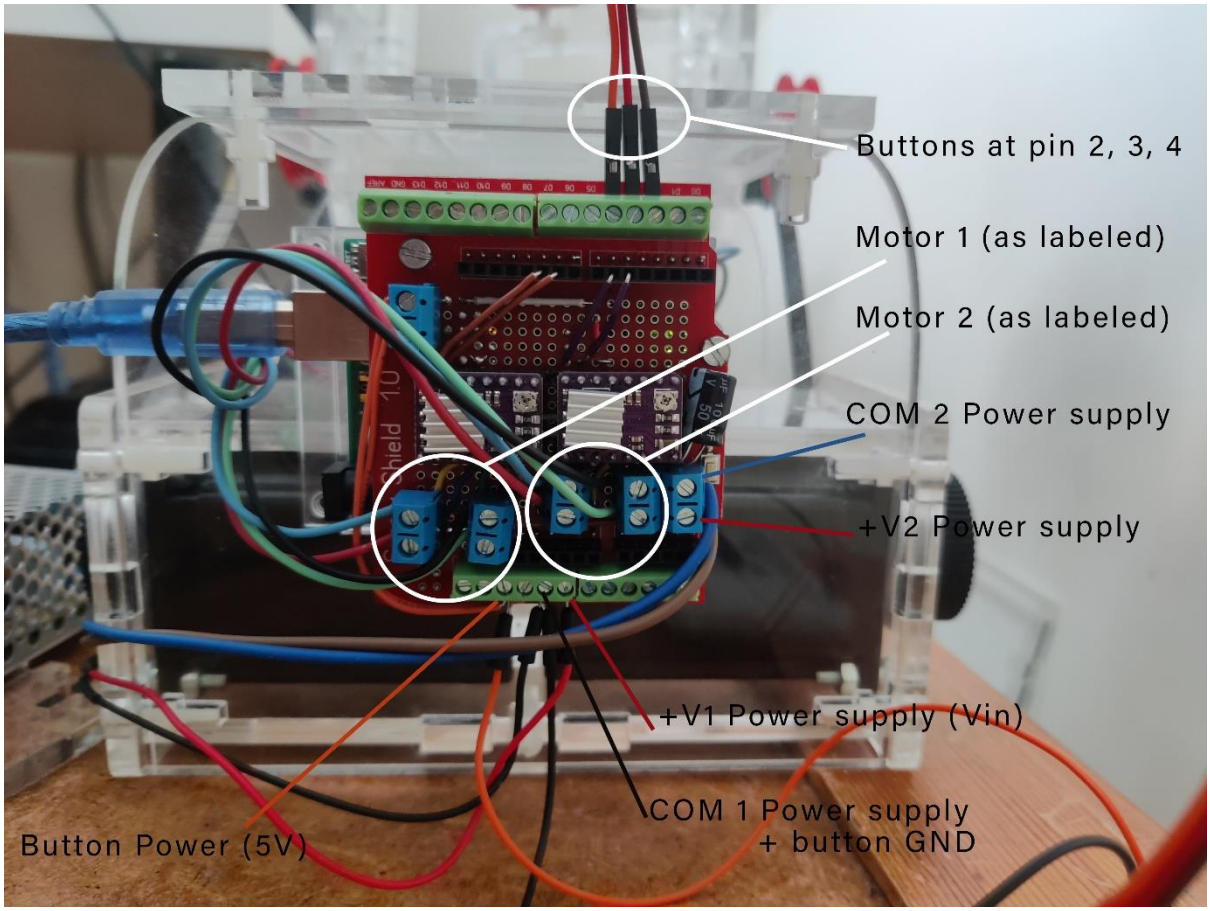

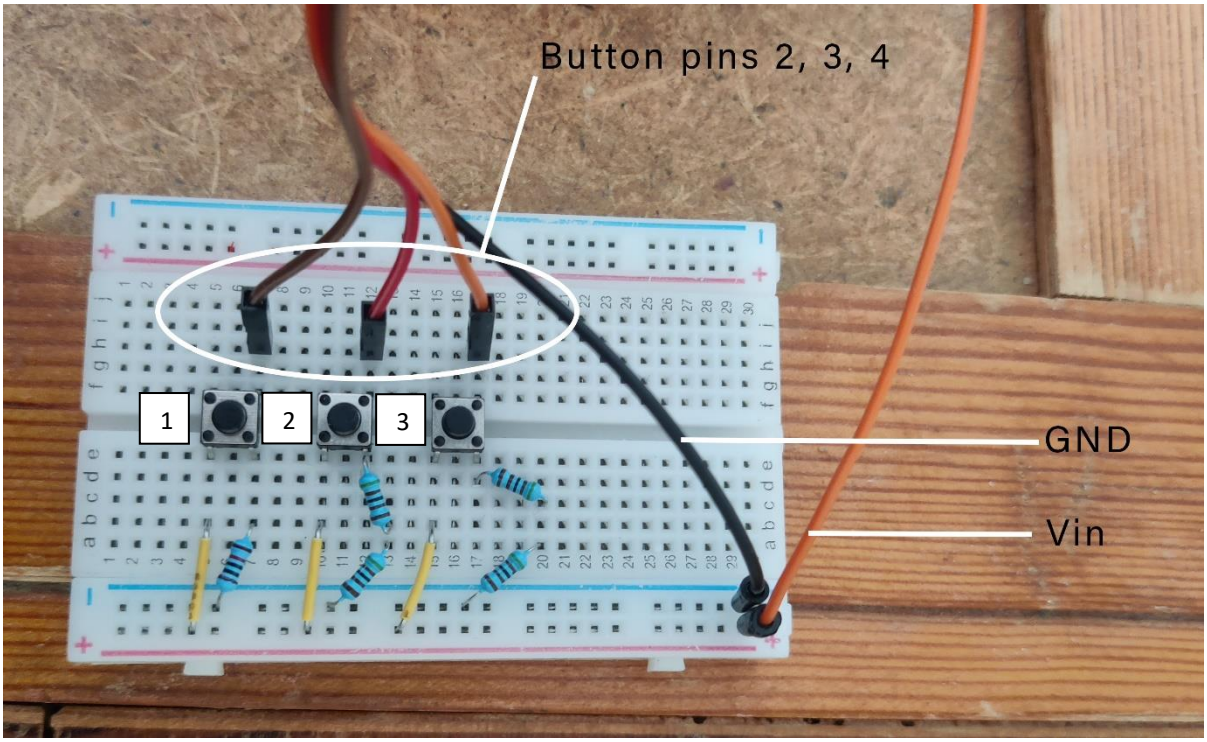

Appendix E, Board placement with tiewraps

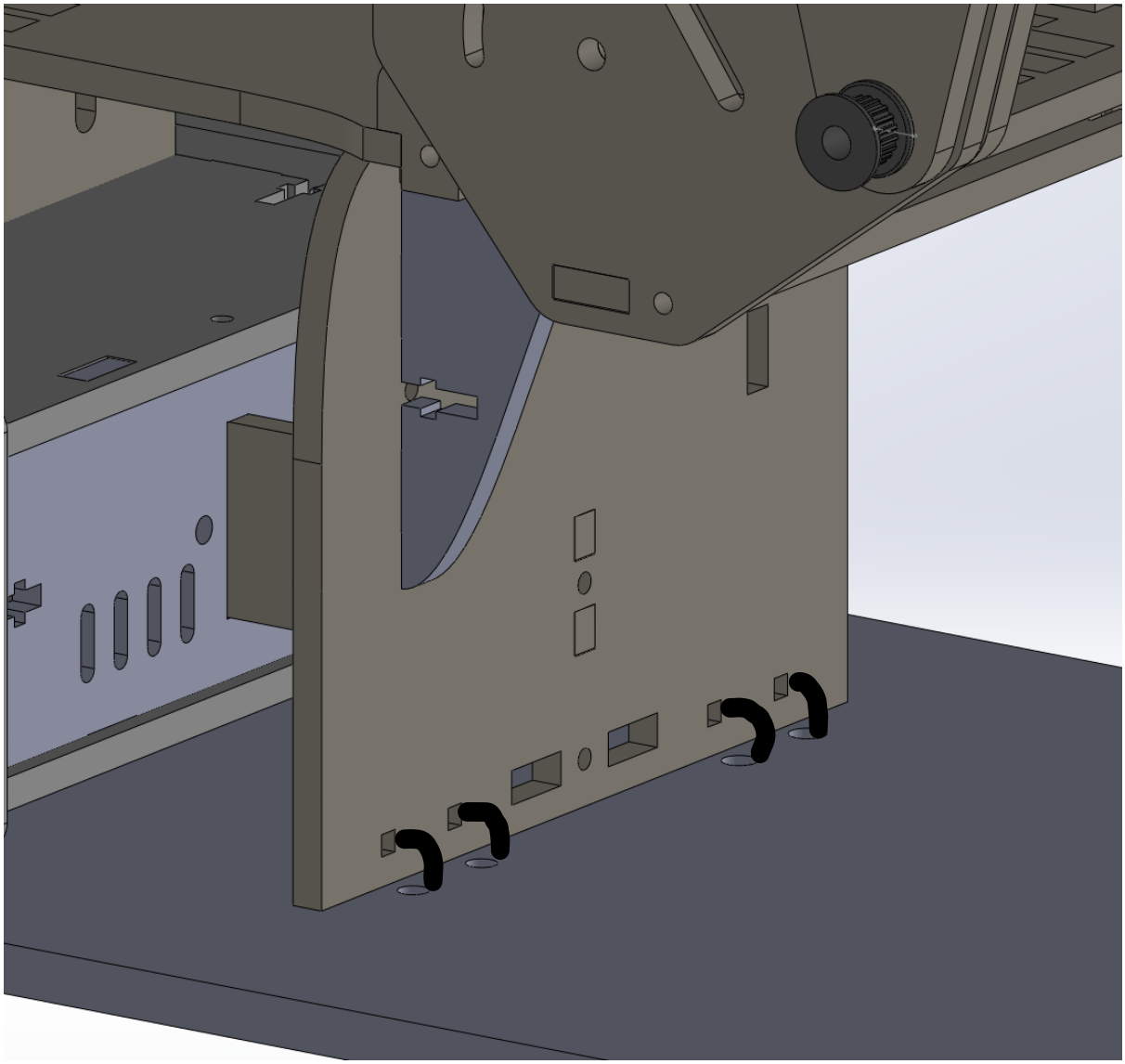

B

ImageJ Macro

```
1
2 //macro to record angle measurement and save image
3
4 macro "Save as Tiff [0]" {
5
6 run("Measure");
7 dir = getDir("image");
8 results_dir = dir + File.separator + "results" + File.separator;
9 fn = getTitle();
10 saveAs("tiff", results_dir + fn);
11
12 run("Open Next");
13
14 }
```